A modified cutting-plane time integration scheme with adaptive substepping for elasto-viscoplastic models

Jian LI[1] and Zhen-Yu YIN[2,*]

[1] Assistant Professor, Key Laboratory of Urban Underground Engineering of Ministry of Education, Beijing Jiaotong Univ., Beijing 100044, China; School of Civil Engineering, Beijing Jiaotong Univ., Beijing 100044, China. Email: jianli@bjtu.edu.cn

[2] Associate Professor, Department of Civil and Environmental Engineering, The Hong Kong Polytechnic Univ., Hung Hom, Kowloon, Hong Kong. (corresponding author) Email: zhenyu.yin@polyu.edu.hk; zhenyu.yin@gmail.com

[*] corresponding author: Dr. Z-Y Yin (Tel: +852 3400 8470; Fax: +852 2334 6389)

Abstract: Integration of stress-strain-time relationship is a key issue for the application of elasto-viscoplastic models to engineering practice. This paper presents a novel adaptive substepping cutting-plane time integration scheme for elasto-viscoplastic models keeping the advantage of original cutting-plane with only the first derivatives of loading surface required. The deficiency of original cutting-plane time integration algorithm is first discussed taking a simple overstress theory based elasto-viscoplastic model EVP-MCC as example. To overcome this, a new algorithm is developed with three features: (1) an evolution function for the hardening variable of dynamic loading surface is innovatively deduced for the Taylor series approximation, (2) the elastic predictor is modified to account for the initial viscoplastic strain rate with more accuracy, and (3) a new adaptive substepping technique for restricting simultaneously both strain and time incremental sizes based on the overstress distance is proposed. For easy understanding, the proposed algorithm is first presented for one-dimensional condition, and then extended to three-dimensional condition. The new integrated EVP-MCC model using the proposed algorithm is examined by simulating laboratory tests at both levels of integration point and finite element with a good performance in terms of accuracy and convergence.

Keywords: viscoplasticity; geomaterials; numerical integration; implicit algorithm; substepping; finite element method

1 Introduction

Numerous experimental studies have revealed the time-dependency of stress-strain behaviours for soils, e.g. creep under constant stress state, stress relaxation under constant strain state, and rate-dependency of strength.[1-7] These time-dependent phenomena of soils lead to many engineering problems, such as long-term settlement and instability of geotechnical structures.[8-11] To consider the time effects in design, elasto-viscoplastic models have been proposed and implemented into finite element codes.[11-19]

The Perzyna's overstress theory[20,21] has been commonly adopted for developing elasto-viscoplastic models. In the overstress approach, the magnitude of a viscoplastic strain-rate is determined by a given overstress function, regarded as an explicit plastic multiplier, representing the distance between a dynamic loading surface and a reference surface. The consistency condition is thus not applied, which is totally different from the plasticity with implied plastic multiplier. Due to this difference, various time integration schemes have been proposed for elasto-viscoplastic models during last decades. For instance, Katona[12] proposed a numerical algorithm employing one-parameter time integration scheme for a viscoplastic cap model and adopted by many researchers.[11,15] His scheme provides an option for explicit or implicit method, in which a Newton-Raphson iteration procedure is applied. Besides, the scheme of Borja and Lee[22] for plasticity was extended by Stolle et al.[14] for an elasto-viscoplastic model, in which the implicit algorithm was realized by a first-order truncated Taylor expansion of the incremental viscoplastic strain rate. However, these algorithms require the secondary derivatives of the yield surface and plastic potential functions for

iteration processes, which lead to tedious numerical implementations.

To seek a simple numerical implementation, the cutting-plane algorithm originally proposed by Ortiz and Simo[13] was extended for an elasto-viscoplastic model of sand by Higgins et al..[16] The integration process of cutting-plane scheme is constituted of an elastic prediction followed by an iterative inelastic correction loop, which is the same as that of other implicit algorithms. Only the first derivatives of yield surface or potential functions are required for iterative inelastic correction loop, which much simplifies the implementation of models. However, the calculation accuracy and convergence of the current cutting-plane algorithm for an elasto-viscoplastic model are poorer than those of other numerical algorithms.[19] The poor performance could be attributed to the fact that the viscoplastic formulation has not been appropriately implemented in this cutting-plane algorithm.

In order to improve the performance of algorithms, the substepping technique can be applied, that is, a given calculation step is divided into several sub-steps with certain criterions. For instance, Bushnell[23] suggested using the value of effective strain increment to determine the number of sub-step. Schreyer[24] proposed a procedure to determine the number of sub-step for an explicit integration algorithm based on the angle between the beginning-of-step and the trial-state unit normal of deviatoric stresses for an isotropic elastic-perfectly plastic von Mises model, which was further extended by Wang et al.[25]. Sloan[26] and Sloan et al.[27] proposed an automatic substepping method, which subdivides the calculation step according to the nonlinear extent of the stress-strain relationship. However, current methods are not applicable for elasto-viscoplastic models which have not only the strain increment but

also time increment with different frameworks from time-independent models.

To keep the advantage of the cutting-plane algorithm with only the first derivatives of loading surface, this paper aims to develop a novel time integration scheme for elasto-viscoplastic models. First, the deficiency of original cutting-plane time integration algorithm is discussed taking a simple elasto-viscoplastic model EVP-MCC as example. Then the first modification is made by deducing an evolution equation of the hardening variable of dynamic loading surface, and a new adaptive substepping procedure for restricting simultaneously both strain and time incremental sizes is proposed to enhance the accuracy and convergence of the algorithm as the second modification. The proposed algorithm is developed and presented from one-dimensional to three-dimensional condition using the EVP-MCC model. The performance of the new algorithm is finally examined by simulating laboratory tests at both integration point and finite element levels.

2 Original cutting-plane time integration algorithm

2.1. General overstress model

According to Perzyna's overstress theory,[20,21] the total strain rate $\dot{\boldsymbol{\varepsilon}}$ is assumed to be consisted of elastic and viscoplastic parts, i.e.,

$$\dot{\boldsymbol{\varepsilon}} = \dot{\boldsymbol{\varepsilon}}^{e} + \dot{\boldsymbol{\varepsilon}}^{vp} \tag{1}$$

where the superscripts *e* and *vp* represent the elastic and the viscoplastic components. The elastic strain rate $\dot{\boldsymbol{\varepsilon}}^{e}$ follows the linear or nonlinear elastic behaviour depending on the material which is generally introduced via elastic modulus. The viscoplastic strain rate $\dot{\boldsymbol{\varepsilon}}^{vp}$ obeys an associated flow rule with respect to the dynamic loading surface f_d. $\dot{\boldsymbol{\varepsilon}}^{e}$ and $\dot{\boldsymbol{\varepsilon}}^{vp}$

could be expressed by:

$$\dot{\boldsymbol{\varepsilon}}^{e} = \boldsymbol{D}^{-1} : \dot{\boldsymbol{\sigma}} \tag{2}$$

$$\dot{\boldsymbol{\varepsilon}}^{vp} = \mu \langle \Phi \rangle \frac{\partial f_d}{\partial \boldsymbol{\sigma}} \tag{3}$$

where $\boldsymbol{D}$ is the elastic matrix; $\boldsymbol{\sigma}$ is stress tensor; μ is the fluidity parameter; Φ is the overstress function representing the distance between the dynamic loading surface and the static yield or reference surface. In soil mechanics, the effective stress tensor defined by $\boldsymbol{\sigma}' = \boldsymbol{\sigma} - u_w \boldsymbol{\delta}$ (where u_w is the pore water pressure and $\boldsymbol{\delta}$ is the Kronecker's delta) is normally used instead of $\boldsymbol{\sigma}$. In elasto-viscoplastic models based on Perzyna's overstress theory, only elastic strain occur when the stress state is inside of the static yield surface[9,28,29]. The static surface can also be replaced by reference surface, due to which viscoplastic strains may occur even though the stress state is inside of the reference surface[10,15,30].

The elapsed time increment for each loading step is assumed to be enough for rate-independent plasticity, which guarantees that the stress state locates on the yield surface during loading process. Therefore, the value of plastic strain increment should be determined by the consistency condition, and the position of the stress state relative to the yield surface should be checked as the completed condition of iterative plastic correction loop. For elasto-viscoplastic models of overstress theory, the elapsed time increment for each loading step is a physical one. Therefore, the determination method of viscoplastic strain rate is different from that of plastic strain increment. According to Eq. (3), the viscoplastic strain rate is obtained by using the overstress function and the first-order derivative of dynamic loading surface as potential surface. Therefore, it is unnecessary for stress state to be located on the static yield

or reference surface, and thus the completed condition of iterative plastic correction loop is totally different from that of rate-independent models.

2.2. Overview of original cutting-plane algorithm

The cutting-plane time integration algorithm extended by Higgins et al.[16] is called original cutting-plane (OCP) algorithm to distinguish the new proposed one in the following sections. The OCP algorithm consists of two basic sequences, i.e. the elastic prediction and the plastic corrector. For easier understanding, a simple elasto-viscoplastic modified Cam-Clay model (EVP-MCC, see Yin et al.[19] and Appendix A) is adopted as example for the presentation. The reference surface is applied for EVP-MCC, which implies the occurring of viscoplastic strains even though the stress state is inside of the reference surface.

A detailed introduction of the original cutting plane algorithm for EVP-MCC could refer to the work by Yin et al.[19]. The flow chart of the OCP is presented in Fig. 1. In the OCP algorithm, the elastic trial stress $\boldsymbol{\sigma}'^{tr}$ is calculated firstly, where the viscoplastic strain rate is assumed to be zero. Then the inelastic correction loop is carried out. The incremental viscoplastic multiplier $\Delta\lambda^i$ is calculated according to the value of overstress function, the first-order derivatives of overstress function and dynamic loading surface (see Fig. 1 where $K_p = (\partial \Phi / \partial p_m^r) h$ with $h = p_m^r[(1+e_0)/(\lambda-\kappa)](\partial f_d / \partial p')$).

$$\Delta\lambda = \frac{\Phi}{\dfrac{\partial \Phi}{\partial \boldsymbol{\sigma}'} \boldsymbol{D} \dfrac{\partial f_d}{\partial \boldsymbol{\sigma}'} - K_p} \tag{4}$$

Subsequently, the stresses and the hardening variable are updated, and the incremental time elapsed within the *i*th iteration of correction loop is determined, where $\bar{t}$ is the

instantaneous time defined by $\bar{t} = \{\mu[(\partial \Phi / \partial \boldsymbol{\sigma}')\boldsymbol{D}(\partial f_d / \partial \boldsymbol{\sigma}') - K_p]\}^{-1}$. Then the summation of the total elapsed time increments $\Sigma \Delta t^i$ is compared with the given time increment Δt as the judgement condition of iterative plastic correction loop with *TTOL* representing the time error tolerance.

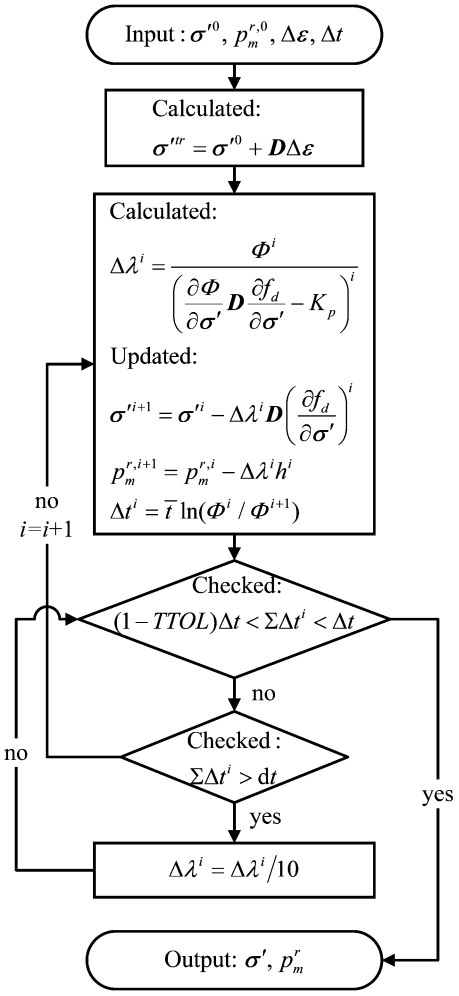

Figure 1 Flow chart of original cutting-plane algorithm with application to EVP-MCC model

2.3. Evaluation of original cutting-plane algorithm under one-dimensional condition

To evaluate the performance of the OCP algorithm, a group of one-dimensional strain-controlled tests, i.e., a compression test and a stress relaxation test, were simulated. For easier understanding, the EVP-MCC model is reduced to one-dimensional condition as presented in Appendix B, and its parameters are summarised in Table 1.

146 **Table 1. Values of initial state parameters and constants of soils**

Parameter	σ_{p0} or p_{m0}^r/kPa	e_0	υ	κ	λ	M_c	$C_{\alpha e}$
Soil for 1D model	50	1.5	0.25	0.01	0.1	-	0.001
Saint-Herblain clay	39	2.26	0.2	0.038	0.48	1.2	0.034

147 The initial stress is 1 kPa for both tests. For the compression test, the specimen was
148 compressed to a strain of 2 % at a strain rate of 1 %/h, and then an additional calculation step
149 with the strain increment $\Delta\varepsilon$ of 0.1 % and Δt of 0.1 h keeping same strain rate was followed
150 to investigate the performance of OCP. For the stress relaxation test, the specimen was firstly
151 compressed to a strain of 1 % at a strain rate of 1 %/h, and then the strain is maintained
152 constant for 100 h. An additional calculation step with the time increment Δt of 1 h was
153 further carried out for stress relaxation to investigate the performance of OCP. To determine
154 the relative error of calculated stress, an ‘‘exact’’ solution σ'_{ex} is required which could be
155 obtained using the enough small strain and time step sizes (10^{-4} % and 10^{-4} h) for the
156 compression stage and small time step size (10^{-2} h) for the relaxation stage. The relative error
157 of stress is computed by $Er = \left|(\sigma' - \sigma'_{ex})/\sigma'_{ex}\right|$.

158 For the additional calculation step of the compression test, the initial stress σ'_0 is 162.52
159 kPa at the strain of 2 %, with the initial hardening parameter σ_p^r of 150.34 kPa. The elastic
160 trial stress σ'^{tr} is firstly calculated using $\Delta\varepsilon$ of 0.1 % and Δt of 0.1 h. Then, the viscoplastic
161 correction is carried out, during which the stress σ' and total accumulated time increment
162 $\Sigma\Delta t^i$ vary with iteration numbers as illustrated in Fig. 2. The total iteration number is 122 for
163 this strain step. The calculated stress decreases from trial value at the beginning of
164 viscoplastic correction procedure, and the total time increment slowly accumulates. Then the
165 calculated stress fluctuates around target stress due to seeking the target total accumulated

time increment. The final updated stress is 167.60 kPa, which has a relative error of 4.34 %.

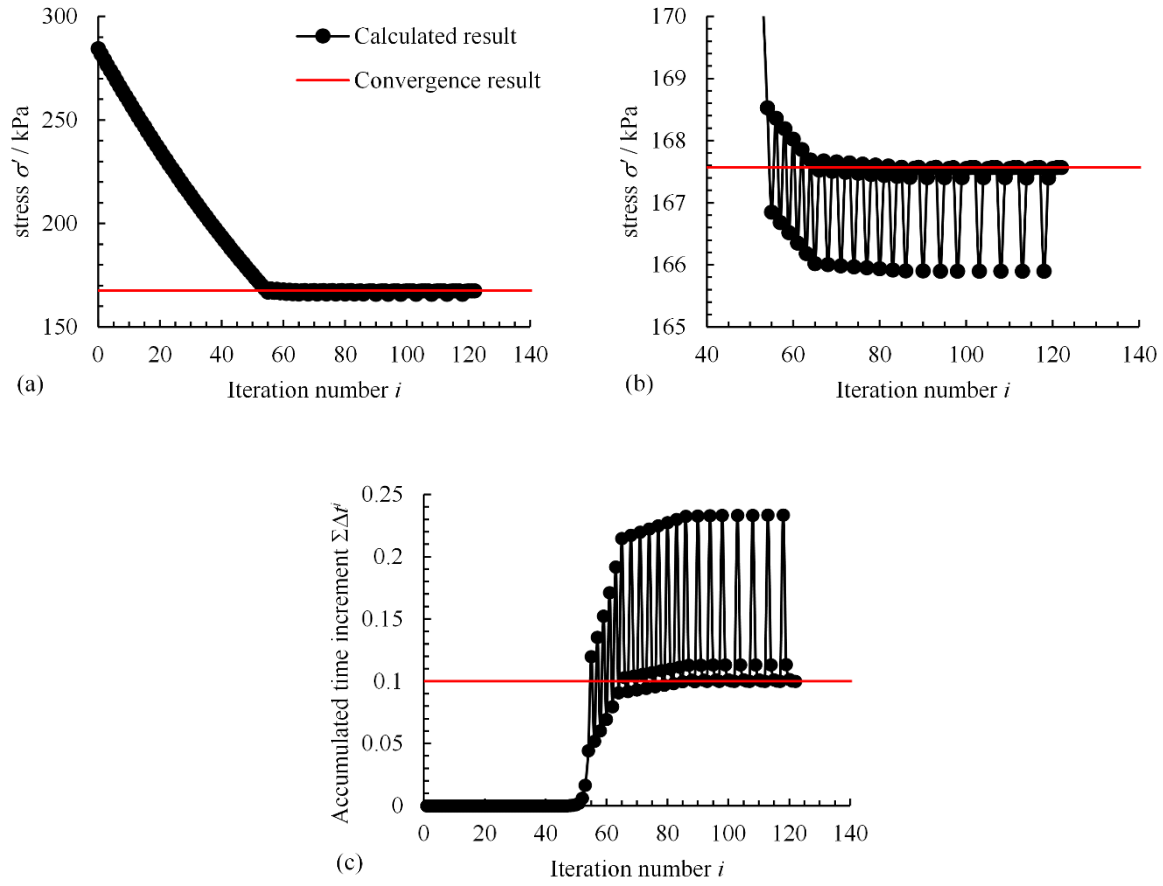

Figure 2 Simulations the one-dimensional compression test by original cutting-plane algorithm: (a) the whole and (b) the partly relationship between stress and iteration number, (c) the relationship between accumulated time increment and iteration number

For the additional calculation step of the stress relaxation test, the initial stress σ'_0 is 68.71 kPa after 100 h of relaxation, with the initial hardening parameter σ_p^r of 71.89 kPa. Because $\Delta\varepsilon$ is equal to zero during relaxation stage, the elastic trial stress σ'^{tr} is equal to the initial one. Then, the viscoplastic correction is carried out for a relaxation of 1 h, during which the stress σ' and total accumulated time increment $\Sigma\Delta t^i$ vary with iteration numbers as illustrated in Fig. 3. The total iteration number is 132 for this step. During the later iterations of stress relaxation stage, the variation of stress is slight. The calculated stress after iteration is 68.71 kPa, which has a slight error. In this case, there is no monotonous reduction

of stress, but significant fluctuation of stress observed towards target stress.

Overall, the above verification shows the performance of OCP algorithm is unsatisfied.

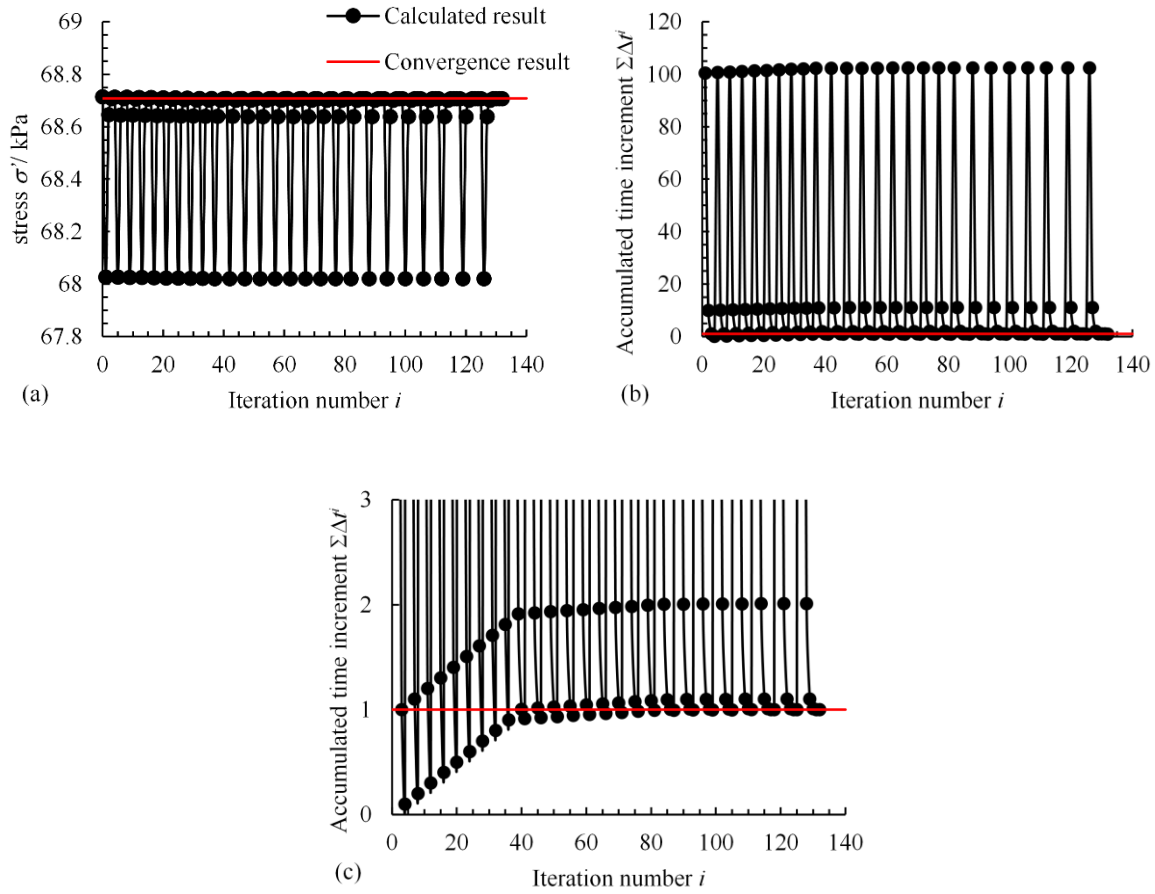

Figure 3 Simulations the one-dimensional stress relaxation test by original cutting-plane algorithm: (a) the relationship between stress and iteration number, (b) the whole and (c) the partly relationship between accumulated time increment and iteration number

2.4. Deficiency of original cutting-plane algorithm

The unsatisfied performance of OCP in terms of calculation accuracy and convergence speed could be ascribed to that the original scheme proposed for plasticity is not appropriate for viscoplasticity. For a cutting-plane algorithm of plasticity, a Taylor series approximation of the yield function f^{i+1} around the current values of yield function f^{i} is required to calculate the change of plastic multiplier of the *i*th iterative plastic correction loop. The target

value of the yield function f^{i+1} could be assumed to be zero. Since the OCP algorithm of viscoplasticity follows the same logic of plasticity, the Taylor series approximation of the overstress function Φ^{i+1} is required to calculate the change of viscoplastic multiplier of the *i*th iterative viscoplastic correction loop, and thus Φ^{i+1} is assumed to be zero as target. However, for a given time increment, the target value of the overstress function Φ^{i+1} is generally not zero depending on the magnitude of time increment. This unrealistic forecast value of overstress function Φ^{i+1} leads to recurrent fluctuations of the calculated stress around target stress up to attaining the target total accumulated time increment (shown in Figs. 2 and 3), due to which the updated stress is inaccurate or/and the convergence is slow.

The above discussion shows that choosing an appropriate function for the Taylor series approximation is vital for the cutting-plane algorithm of viscoplasticity. An appropriate function should have two features: (1) Its target value is known. In viscoplasticity the target value of reference surface function f_r^{i+1} is unknown during iterative viscoplastic correction loop, and thus f_r is inappropriate. (2) The variables in the function are independent. In the OCP algorithm both σ' and σ_p^d are variables in the dynamic loading function f_d. σ_p^d is directly solved from the stress state according to $f_d = 0$, and thus it is not independent. Therefore, f_d seems to be inappropriate either.

3 New time integration scheme for one-dimensional condition

3.1. Modification of cutting-plane algorithm

As discussed above, it is important to find a function with known target value and independent variables for the correct cutting-plane time integration algorithm. In elasto-

viscoplastic models of overstress theory, the overstress function is adopted to calculate the viscoplastic multiplier rate, i.e., Eq. (3). Taking the one-dimensional model of EVP-MCC (see Appendix B) as example, the viscoplastic multiplier rate could be expressed by:

$$\dot{\lambda} = \mu \langle \Phi \rangle = \mu \left(\frac{\sigma_p^d}{\sigma_p^r} \right)^{\beta} \tag{5}$$

Using Eq. (5), σ_p^d could be expressed by:

$$\sigma_p^d = \sigma_p^r \left(\frac{\dot{\lambda}}{\mu} \right)^{1/\beta} \tag{6}$$

Then, Eq. (6) indicates that the σ_p^d could be calculated independently without using the stress σ'. In this case, the f_d becomes a function with known target value ($f_d = 0$) and having independent variables (σ_p^d not directly from σ').

The increment of σ_p^d could be calculated by:

$$\mathrm{d}\sigma_p^d = \frac{\partial \sigma_p^d}{\partial \dot{\lambda}} \mathrm{d}\dot{\lambda} + \frac{\partial \sigma_p^d}{\partial \sigma_p^r} \mathrm{d}\sigma_p^r = \frac{\partial \sigma_p^d}{\partial \dot{\lambda}} \mathrm{d}\dot{\lambda} + \frac{\partial \sigma_p^d}{\partial \sigma_p^r} \frac{\partial \sigma_p^r}{\partial \varepsilon^{vp}} \mathrm{d}\lambda \frac{\partial f_d}{\partial \sigma} \tag{7}$$

where $\mathrm{d}\dot{\lambda}$ is viscoplastic multiplier rate increment, $\mathrm{d}\lambda$ is viscoplastic multiplier increment, and

$$\mathrm{d}\lambda = \dot{\lambda} \mathrm{d}t \tag{8}$$

Then the consistency condition for the dynamic loading surface is given by:

$$\begin{aligned} \mathrm{d}f_d &= \frac{\partial f_d}{\partial \sigma'} \mathrm{d}\sigma' + \frac{\partial f_d}{\partial \sigma_p^d} \mathrm{d}\sigma_p^d \\ &= \frac{\partial f_d}{\partial \sigma'} E \left(\mathrm{d}\varepsilon - \dot{\lambda} \mathrm{d}t \frac{\partial f_d}{\partial \sigma'} \right) + \frac{\partial f_d}{\partial \sigma_p^d} \frac{\partial \sigma_p^d}{\partial \dot{\lambda}} \mathrm{d}\dot{\lambda} + \frac{\partial f_d}{\partial \sigma_p^d} \frac{\partial \sigma_p^d}{\partial \sigma_p^r} \frac{\partial \sigma_p^r}{\partial \varepsilon^{vp}} \dot{\lambda} \mathrm{d}t \frac{\partial f_d}{\partial \sigma'} = 0 \end{aligned} \tag{9}$$

and then $\mathrm{d}\dot{\lambda}$ could be obtained, expressed by:

$$
\begin{aligned}
\mathrm{d}\dot{\lambda} &= \frac{\dfrac{\partial f_d}{\partial \sigma'} E \mathrm{d}\varepsilon - \dot{\lambda}\left(\dfrac{\partial f_d}{\partial \sigma'} E \dfrac{\partial f_d}{\partial \sigma'} - \dfrac{\partial f_d}{\partial \sigma_p^d} \dfrac{\partial \sigma_p^d}{\partial \sigma_p^r} \dfrac{\partial \sigma_p^r}{\partial \varepsilon^{vp}} \dfrac{\partial f_d}{\partial \sigma'} \right) \mathrm{d}t}{-\dfrac{\partial f_d}{\partial \sigma_p^d} \dfrac{\partial \sigma_p^d}{\partial \dot{\lambda}}} \\
&= \frac{E \mathrm{d}\varepsilon - \dot{\lambda}\left[E + \left(\dfrac{\dot{\lambda}}{\mu} \right)^{1/\beta} \dfrac{\sigma_p^r (1+e_0)}{\lambda - \kappa} \right] \mathrm{d}t}{\dfrac{\sigma_p^d}{\beta \dot{\lambda}}}
\end{aligned}
\tag{10}
$$

Eq. (10) implies that the value of $\mathrm{d}\dot{\lambda}$ is dependent not only on the strain increment $\mathrm{d}\varepsilon$ but also on the time increment $\mathrm{d}t$.

3.2. Modification of elastic predictor

Based on the above re-arranged elasto-viscoplastic formulations, a modified cutting-plane (MCP) algorithm could be proposed. In finite element analysis, the initial stress and hardening variables are known for each Gauss point, and the new stress and hardening variables require to be updated by the integration for given increments of strain and time. The algorithm herein follows this logic, which is similar to other implicit schemes, the MCP uses predictor with an iterative correction loop for given increments of strain and time.

For implicit schemes of elastoplasticity or the OCP scheme of viscoplasticity, the total strain increment is assumed to be completely elastic as predictor (so-called “elastic predictor”), and the inelastic strain increment or the viscoplastic multiplier increment (Eq. (4)) is determined during the correction iteration. Different from this, in the MCP scheme of viscoplasticity the viscoplastic multiplier *rate* increment (Eq. (10)) is determined during the correction iteration. Furthermore, different from elastoplasticity, at any step before loading (i.e. initial state) in viscoplasticity it exists a viscoplastic strain-rate (see Eq. (3)) which

should be considered in the elastic predictor to be more accurate and more consistent with the viscoplastic multiplier *rate* increment.

Thus, for a given Δt , the initial values of viscoplastic multiplier rate $\dot{\lambda}^0$ and viscoplastic multiplier increment $\mathrm{d}\lambda^0$ are given by:

$$\dot{\lambda}^0 = \mu \left(\frac{\sigma_p^{d,0}}{\sigma_p^{r,0}} \right)^{\beta} \tag{11}$$

$$\mathrm{d}\lambda^0 = \dot{\lambda}^0 \Delta t \tag{12}$$

where $\sigma_p^{d,0}$ and $\sigma_p^{r,0}$ are initial values before loading.

Different from elastic trial stress, the more accurate trial stress σ'^{tr} is then expressed by:

$$\sigma'^{tr} = \sigma'^0 + E\left(\Delta\varepsilon - \mathrm{d}\lambda^0 \frac{\partial f_d}{\partial \sigma'} \right) = \sigma'^0 + E(\Delta\varepsilon - \mathrm{d}\lambda^0) \tag{13}$$

Similar to the modification logic of trial stress, the hardening variables $\sigma_p^{d,tr}$ and $\sigma_p^{r,tr}$ should also account for the initial viscoplastic strain-rate, and are expressed by:

$$\sigma_p^{d,tr} = \sigma_p^{d,0} + \frac{\partial \sigma_p^d}{\partial \sigma_p^r} \frac{\partial \sigma_p^r}{\partial \varepsilon^{vp}} \mathrm{d}\lambda^0 \frac{\partial f_d}{\partial \sigma'} = \sigma_p^{d,0} + \left(\frac{\dot{\lambda}}{\mu} \right)^{1/\beta} \frac{\sigma_p^r (1+e_0)}{\lambda - \kappa} \mathrm{d}\lambda^0 \tag{14}$$

$$\sigma_p^{r,tr} = \sigma_p^{r,0} + \frac{\partial \sigma_p^r}{\partial \varepsilon^{vp}} \mathrm{d}\lambda^0 \frac{\partial f_d}{\partial \sigma'} = \sigma_p^{r,0} + \frac{\sigma_p^r (1+e_0)}{\lambda - \kappa} \mathrm{d}\lambda^0 \tag{15}$$

The position of the stress state relative to the dynamic loading surface is determined by calculating the dynamic loading surface function f_d^{tr} using updated values of Eqs. (13) and (14). The value of the function f_d^{tr} is checked against the dynamic loading surface error tolerance *FTOL*, where *FTOL* is a small positive number. If the stress state sufficiently close to the dynamic loading surface such as $| f_d^{tr} | \leq FTOL$, the calculated stress and hardening variables are accepted and the calculation step is completed. Otherwise, the stress state is far

away from the dynamic loading surface (| f_d^{tr} |>*FTOL*), and then the calculation enters into an iterative viscoplastic correction loop.

3.3. Viscoplastic correction loop

For a viscoplastic correction loop, the increment of viscoplastic multiplier rate $\mathrm{d}\dot{\lambda}$ could be calculated using a Taylor series approximation of the dynamic loading function:

$$\begin{aligned} f_d^{i+1} &= f_d^i + \left(\frac{\partial f_d}{\partial \sigma'}\right)^i \mathrm{d}\sigma'^i + \left(\frac{\partial f_d}{\partial \sigma_p^d}\right)^i \mathrm{d}\sigma_p^{d,i} \\ &= f_d^i - \left(\frac{\partial f_d}{\partial \sigma'}\right)^i E \left(\frac{\partial f_d}{\partial \sigma'}\right)^i \mathrm{d}\dot{\lambda}^i \Delta t + \left(\frac{\partial f_d}{\partial \sigma_p^d}\frac{\partial \sigma_p^d}{\partial \dot{\lambda}}\right)^i \mathrm{d}\dot{\lambda}^i + \left(\frac{\partial \sigma_p^d}{\partial \sigma_p^r}\frac{\partial \sigma_p^r}{\partial \varepsilon^{vp}}\frac{\partial f_d}{\partial \sigma'}\right)^i \mathrm{d}\dot{\lambda}^i \Delta t \end{aligned} \tag{16}$$

For each step, the stress state should return back to the dynamic loading surface. Thus, the target value of the dynamic loading function f_d^{i+1} is set to zero. Based on it, the value of $\mathrm{d}\dot{\lambda}$ is computed by:

$$\begin{aligned} \mathrm{d}\dot{\lambda}^i &= \frac{f_d^i}{\left(\frac{\partial f_d}{\partial \sigma'} E \frac{\partial f_d}{\partial \sigma'} - \frac{\partial \sigma_p^d}{\partial \sigma_p^r}\frac{\partial \sigma_p^r}{\partial \varepsilon^{vp}}\frac{\partial f_d}{\partial \sigma'}\right)^i \Delta t - \left(\frac{\partial f_d}{\partial \sigma_p^d}\frac{\partial \sigma_p^d}{\partial \dot{\lambda}}\right)^i} \\ &= \frac{f_d^i}{\left[E - \left(\frac{\dot{\lambda}}{\mu}\right)^{1/\beta} \frac{\sigma_p^r (1+e_0)}{\lambda - \kappa}\right]^i \Delta t + \left(\frac{\sigma_p^d}{\beta \dot{\lambda}}\right)^i} \end{aligned} \tag{17}$$

Because $\mathrm{d}\dot{\lambda}$ is calculated by taking an approximation of f_d, the correction loop may take several iterations to bring the stress state back to the dynamic loading surface which is simultaneously developing with σ_p^d. With the new $\mathrm{d}\dot{\lambda}$, the stress and hardening variables are updated by:

$$\sigma'^{i+1} = \sigma'^i - \mathrm{d}\dot{\lambda}^i \Delta t E \frac{\partial f_d}{\partial \sigma'} = \sigma'^i - \mathrm{d}\dot{\lambda}^i \Delta t E \tag{18}$$

$$\sigma_m^{d,i+1} = \sigma_m^{d,i} + \left(\frac{\partial \sigma_p^d}{\partial \dot{\lambda}}\right)^i \mathrm{d}\dot{\lambda}^i + \left(\frac{\partial \sigma_p^d}{\partial \sigma_p^r}\frac{\partial \sigma_p^r}{\partial \varepsilon^{vp}}\frac{\partial f_d}{\partial \sigma'}\right)^i \mathrm{d}\dot{\lambda}^i \Delta t$$

$$= \sigma_m^{d,i} + \left(\frac{\sigma_p^d}{\beta \dot{\lambda}}\right)^i \mathrm{d}\dot{\lambda}^i + \left[\left(\frac{\dot{\lambda}}{\mu}\right)^{1/\beta} \frac{\sigma_p^r (1+e_0)}{\lambda - \kappa}\right]^i \mathrm{d}\dot{\lambda}^i \Delta t \quad (19)$$

$$\sigma_p^{r,i+1} = \sigma_p^{r,i} + \left(\frac{\partial \sigma_p^r}{\partial \varepsilon^{vp}}\right)^i \mathrm{d}\dot{\lambda}^i \Delta t \frac{\partial f_d}{\partial \sigma'} = \sigma_p^{r,i} + \left[\frac{\sigma_p^r (1+e_0)}{\lambda - \kappa}\right]^i \mathrm{d}\dot{\lambda}^i \Delta t \quad (20)$$

During the iteration, the value of the dynamic loading function f_d^{i+1} is checked. If the stress state is far away from the dynamic loading surface ($|f_d^{i+1}| > FTOL$), the correction loop will iterate again. If the stress state is on or nearby the dynamic loading surface ($|f_d^{i+1}| \leq FTOL$), the iterative loop is completed, and the updated stress and hardening variables are recorded as the initial state of next loading step.

For easier understanding, the integration process of the proposed MCP algorithm for one arbitrary loading step is illustrated as follows:

(1) Calculate $\dot{\lambda}^0$ and $\mathrm{d}\lambda^0$ by Eqs. (11) and (12), and then update σ'^{tr}, $\sigma_p^{d,tr}$ and $\sigma_p^{r,tr}$ by Eqs. (13)-(15).

(2) Check f_d^{tr}, enter iterative viscoplastic correction loop if $|f_d^{tr}| > FTOL$, otherwise complete the loading step.

(3) Calculate $\mathrm{d}\dot{\lambda}^i$ by Eq. (17) if $|f_d^{tr}| > FTOL$, and then update σ'^{i+1}, $\sigma_p^{d,i+1}$ and $\sigma_p^{r,i+1}$ by Eqs. (18)-(20).

(4) Check f_d^{i+1}, enter the next iterative viscoplastic correction loop if $|f_d^{i+1}| > FTOL$, otherwise complete the loading step.

3.4. Adaptive substepping technique for viscoplasticity

The stress-strain relationship is generally nonlinear for viscoplasticity. For a given initial

293 stress state, the unknown values of stress and hardening variables are highly dependent on
294 increments of strain and time. This may lead to calculation error which could not be
295 absolutely eliminated regardless of using explicit or implicit algorithms. In fact, this
296 calculation error or non-convergence could be controlled by decreasing the loading step size
297 for both explicit and implicit algorithms.[23-27] Besides, an appropriate step size is also needed
298 for implicit algorithm to guarantee convergence. In principle, the iteration process easily
299 converges if a sufficiently good initial guess is supplied. But it can still fail to converge if
300 putative root does not exist nearby. This problem of convergence could be efficiently solved
301 by limiting the maximum loading step size.

302 According to the above discussion, the performance of an algorithm, i.e., accuracy and
303 convergence, gradually deteriorates with the increasing of loading step size. Therefore, it is
304 necessary to conditionally limit the maximum loading step size. The substepping procedure
305 for viscoplastic models was rarely mentioned in the literature. Different from elastoplasticity,
306 the loading step size is controlled by not only $\Delta\varepsilon$ but also Δt for the viscoplasticity, due to
307 which a new substepping scheme should be proposed. According to the framework of
308 overstress theory, the loading step size could be represented by the distance between the trial
309 stress and dynamic loading surface adjusted on the prediction stage, where the positions of
310 trial stress and dynamic loading surface shift with $\Delta\varepsilon$ and Δt, respectively. This distance
311 could be expressed by:

312 $$\mathrm{d}\bar{\sigma}'^{tr} = \sigma'^{tr} - \sigma_p^{dtr} \tag{21}$$

313 Comparing to the initial stress state, the ratio *k'* representing how relatively small the current

step size can be estimated by:

$$\mathrm{d}\bar{\sigma}'^{tr} = k'\sigma'^{tr} \quad \text{or} \quad k' = \mathrm{d}\bar{\sigma}'^{tr} \big/ \sigma'^{tr} \tag{22}$$

To control the substepping size, a substepping parameter k given by users is introduced. If $k' \le k$ representing that the current step size is small enough as expected, no substepping is required. Otherwise, a substepping is needed for which α_j representing the size ratio of substepping at current loading step with its range from 0 to 1 is introduced to calculate the sub-step sizes $\alpha_j \Delta\varepsilon$ and $\alpha_j \Delta t$, where the subscript j counts the number of the substepping. In order to have an adoptive substepping, the value of α_j is estimated by Eq.(23) to make sure that the new sub-step size is within that of expected maximum value,

$$\alpha_j = k\bar{\sigma}_j'^{tr} \big/ \mathrm{d}\bar{\sigma}_j'^{tr} \tag{23}$$

An adaptive substepping procedure for one loading step is then proposed for a given substepping parameter k, shown as follows:

(1) Set initial value of $\alpha_j = 1$ for j = 1.

(2) Calculate $\sigma_j'^{tr}$, $\sigma_{p,j}^{d,tr}$ and $\sigma_{p,j}^{r,tr}$ by using $\alpha_j \Delta\varepsilon$ and $\alpha_j \Delta t$, then calculate $\mathrm{d}\bar{\sigma}_j'^{tr}$ by $\sigma_{p,j}^{d,tr}$.

(3) Compare $\mathrm{d}\bar{\sigma}_j'^{tr}$ and $\sigma_j'^{tr}$. If $\mathrm{d}\bar{\sigma}_j'^{tr} \big/ \sigma_j'^{tr} > k$, α_j is adjusted by $\alpha_j = k\sigma_j'^{tr} \big/ \mathrm{d}\bar{\sigma}_j'^{tr}$, and return back to (2) to re-calculate trial stress and hardening variables.

(4) Calculate σ_j', $\sigma_{p,j}^{d}$ and $\sigma_{p,j}^{r}$ by viscoplastic correction.

(5) Check $\sum_j \alpha_j = 1$. If yes, the calculation is completed; otherwise, $\alpha_{j+1} = 1 - \Sigma\alpha_j$, return to (2).

To clarify the whole algorithm, the flow chart of the new MCP algorithm with the adaptive substepping procedure for one-dimensional condition is presented in Fig. 4.

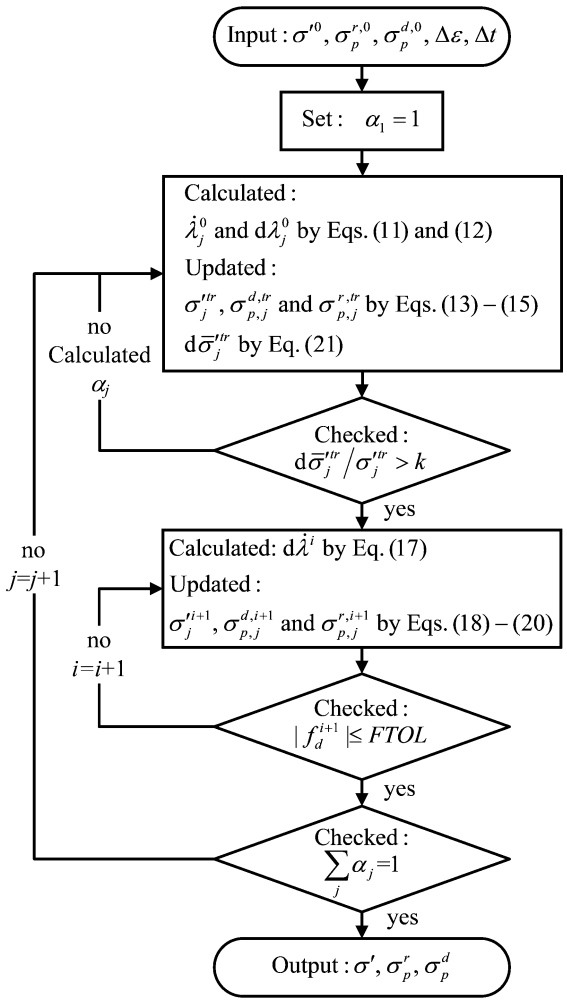

Figure 4 Flow chart of modified cutting-plane algorithm for one-dimensional EVP-MCC model

3.5. Performance of modified cutting-plane algorithm

To investigate the performance of MCP algorithm, the same group of one-dimension strain-controlled tests, i.e., the compression test and the stress relaxation test, were simulated firstly by the one-dimensional EVP-MCC model using MCP without substepping procedure. Because the first derivatives of loading surface are constant for one-dimension condition, only one iteration is needed during viscoplastic correction stage for MCP. The relative errors for two selected calculation steps are 0.267 % and less than 0.0001 %, respectively, for the compression test and the stress relaxation test. This illustrates that the performance of the MCP algorithm is better than that of the OCP algorithm.

Moreover, a series of one-dimensional compression tests with large changes of strain rate was simulated by the MCP algorithm without substepping. The test scheme is the same as the former one, except that the additional calculation step of $\Delta\varepsilon$ of 0.1 % was conducted at different strain rates $\dot{\varepsilon}$ (i.e., 0.01 %/h, 0.1 %/h, 1 %/h, 10 %/h and 100 %/h) implying different time increments. The variation of calculated stress error *Er* with strain rate $\dot{\varepsilon}$ is illustrated in Fig. 5, which shows a decrease followed by an increase of *Er* with the increase of strain rate. The large error of stress is attributed to that the value of initial viscoplastic strain rate determined by the initial stress state deviates from the actual value of the loading step even through the time increment is small.

Two one-dimensional compression tests with two largest changes of strain rate (i.e., 0.01 %/h and 100 %/h) were simulated by the MCP algorithm with different substepping parameters (i.e., k = 0.05, 0.1, 0.2 and 0.5) to investigate the ability of the proposed substepping technique. The variations of iteration number N and relative error of calculated stress *Er* with substepping parameter k are illustrated in Fig. 6. The iteration number N slightly decreases with the increasing of k for the situation of changing $\dot{\varepsilon}$ from 1 %/h to 0.01 %/h, while N increases with the increasing of k for the situation of changing $\dot{\varepsilon}$ from 1 %/h to 100 %/h. The relative errors of stress *Er* increase with the increasing of k for both cases. Moreover, the values of *Er* for both cases are similar when k = 0.05 and 0.1, however, the value of *Er* for the case of changing $\dot{\varepsilon}$ from 1 %/h to 100 %/h is significantly greater than that of changing $\dot{\varepsilon}$ from 1 %/h to 0.01 %/h when k = 0.5.

For the case of changing $\dot{\varepsilon}$ from 1 %/h to 0.01 %/h, the strain rate reduces by 100 times;

for the case of changing $\dot{\varepsilon}$ from 1 %/h to 100 %/h, the strain rate increases by 100 times. The viscoplastic strain increment for the former case is significantly smaller than that for the latter with the same strain increment $\Delta\varepsilon$ but different time increment Δt. According to the variations of *N* and *Er* with *k*, it is found that the performance of accuracy is much improved by the substepping technique for simulations with large change of strain rate. The effects of the substepping parameter *k* on the iteration number *N* and the relative error of stress *Er* are significant indicating that the value of *k* should be carefully selected.

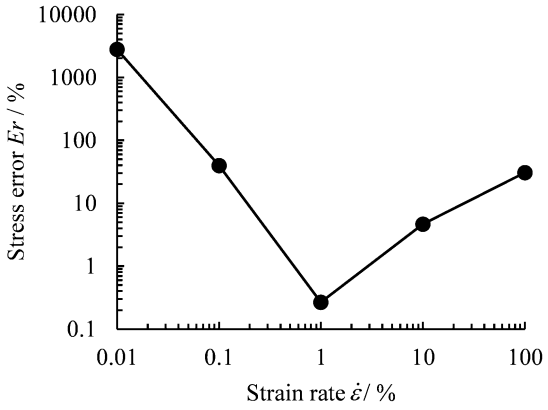

Figure 5 Variation of relative error of stress with strain rate of tested calculation step for one-dimensional compression test.

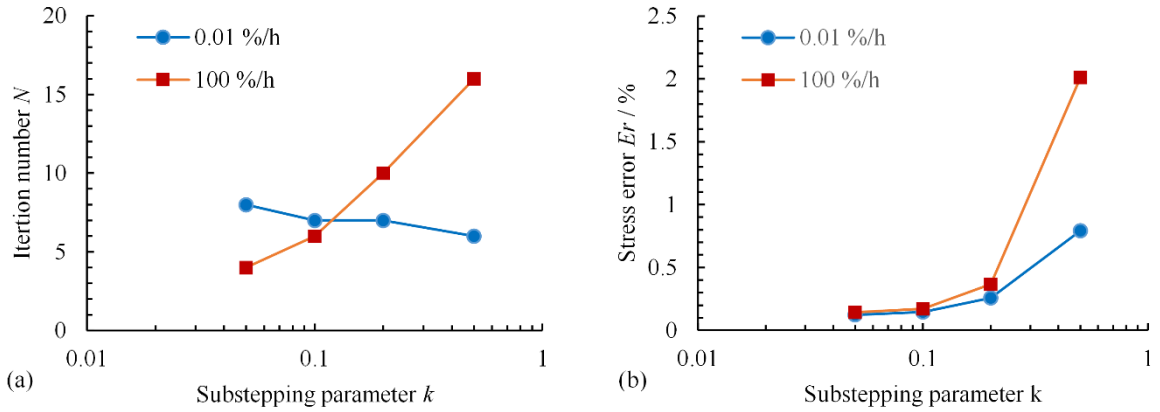

Figure 6 Variation of (a) iteration number and (b) relative error of stress with substepping parameter for one-dimensional compression test at strain rates of 0.01 %/h and 100 %/h of tested step.

4 New time integration scheme for three-dimensional condition

The proposed MCP algorithm is further applied to the three-dimensional EVP-MCC (Appendix A). The scheme of MCP algorithm for three-dimensional model is same as that for one-dimensional model. Only the difference of MCP application between three-dimensional and one-dimensional conditions is presented in this section.

The consistency condition for the dynamic loading surface of three-dimensional EVP-MCC is given by:

$$\begin{aligned} \mathrm{d}f_d &= \frac{\partial f_d}{\partial \boldsymbol{\sigma}'} : \mathrm{d}\boldsymbol{\sigma}' + \frac{\partial f_d}{\partial p_m^d}\mathrm{d}p_m^d \\ &= \frac{\partial f_d}{\partial \boldsymbol{\sigma}'} : \boldsymbol{D} : \left(\mathrm{d}\boldsymbol{\varepsilon} - \dot{\lambda}\mathrm{d}t \frac{\partial f_d}{\partial \boldsymbol{\sigma}'} \right) + \frac{\partial f_d}{\partial p_m^d}\frac{\partial p_m^d}{\partial \dot{\lambda}}\mathrm{d}\dot{\lambda} + \frac{\partial f_d}{\partial p_m^d}\frac{\partial p_m^d}{\partial p_m^r}\frac{\partial p_m^r}{\partial \varepsilon_v^{vp}}\dot{\lambda}\mathrm{d}t\frac{\partial f_d}{\partial p'} = 0 \end{aligned} \tag{24}$$

and $\mathrm{d}\dot{\lambda}$ could be obtained, expressed by:

$$\mathrm{d}\dot{\lambda} = \frac{\dfrac{\partial f_d}{\partial \boldsymbol{\sigma}'}\boldsymbol{D} : \mathrm{d}\boldsymbol{\varepsilon} - \dot{\lambda}\left(\dfrac{\partial f_d}{\partial \boldsymbol{\sigma}'} : \boldsymbol{D} : \dfrac{\partial f_d}{\partial \boldsymbol{\sigma}'} - \dfrac{\partial f_d}{\partial p_m^d}\dfrac{\partial p_m^d}{\partial p_m^r}\dfrac{\partial p_m^r}{\partial \varepsilon_v^{vp}}\dfrac{\partial f_d}{\partial p'} \right)\mathrm{d}t}{-\dfrac{\partial f_d}{\partial p_m^d}\dfrac{\partial p_m^d}{\partial \dot{\lambda}}} \tag{25}$$

with

$$\frac{\partial f_d}{\partial \boldsymbol{\sigma}'} = \frac{\partial f_d}{\partial \boldsymbol{\sigma}_d'} : \frac{\partial \boldsymbol{\sigma}_d'}{\partial \boldsymbol{\sigma}'} + \frac{\partial f_d}{\partial p'}\frac{\partial p'}{\partial \boldsymbol{\sigma}'}$$

$$\frac{\partial f_d}{\partial \boldsymbol{\sigma}_d'} = \frac{3\boldsymbol{\sigma}_d'}{M^2 p'}; \quad \frac{\partial \boldsymbol{\sigma}_d'}{\partial \boldsymbol{\sigma}'} = \begin{bmatrix} \frac{2}{3} & -\frac{1}{3} & -\frac{1}{3} & 0 & 0 & 0 \\ -\frac{1}{3} & \frac{2}{3} & -\frac{1}{3} & 0 & 0 & 0 \\ -\frac{1}{3} & -\frac{1}{3} & \frac{2}{3} & 0 & 0 & 0 \\ 0 & 0 & 0 & \sqrt{2} & 0 & 0 \\ 0 & 0 & 0 & 0 & \sqrt{2} & 0 \\ 0 & 0 & 0 & 0 & 0 & \sqrt{2} \end{bmatrix} \tag{26}$$

$$\frac{\partial f_d}{\partial p'} = -\frac{\frac{3}{2}\boldsymbol{\sigma}_d' : \boldsymbol{\sigma}_d'}{M^2 p'^2} + 1; \quad \frac{\partial p'}{\partial \boldsymbol{\sigma}'} = \left[\tfrac{1}{3}, \tfrac{1}{3}, \tfrac{1}{3}, 0, 0, 0\right]^T$$

$$\frac{\partial f_d}{\partial p_m^d} = -1; \quad \frac{\partial p_m^d}{\partial p_m^r} = \left(\frac{\dot{\lambda}}{\mu}\right)^{1/\beta}; \quad \frac{\partial p_m^r}{\partial \varepsilon_v^{vp}} = \frac{p_m^r(1+e_0)}{\lambda - \kappa}; \quad \frac{\partial p_m^d}{\partial \dot{\lambda}} = \frac{p_m^d}{\beta\dot{\lambda}}$$

During the predictor stage at the beginning of calculation step, the trial stress $\boldsymbol{\sigma}'^{tr}$ could be expressed by:

$$\boldsymbol{\sigma}'^{tr} = \boldsymbol{\sigma}'^{0} + \boldsymbol{D} : \left(\Delta\boldsymbol{\varepsilon} - \mathrm{d}\lambda^{0} \frac{\partial f_d}{\partial \boldsymbol{\sigma}'} \right) \tag{27}$$

The hardening variables $p_m^{d,tr}$ and $p_m^{r,tr}$ could be expressed by:

$$p_m^{d,tr} = p_m^{d,0} + \frac{\partial p_m^d}{\partial p_m^r} \frac{\partial p_m^r}{\partial \varepsilon_v^{vp}} \mathrm{d}\lambda^{0} \frac{\partial f_d}{\partial p'} \tag{28}$$

$$p_m^{r,tr} = p_m^{r,0} + \frac{\partial p_m^r}{\partial \varepsilon_v^{vp}} \mathrm{d}\lambda^{0} \frac{\partial f_d}{\partial p'} \tag{29}$$

For the correction loop, the Taylor series approximation of the dynamic loading function is expressed by:

$$\begin{aligned} f_d^{i+1} &= f_d^i + \left(\frac{\partial f_d}{\partial \boldsymbol{\sigma}'} \right)^i : \mathrm{d}\boldsymbol{\sigma}'^{i} + \left(\frac{\partial f_d}{\partial p_m^d} \right)^i \mathrm{d}p_m^{d,i} \\ &= f_d^i - \left(\frac{\partial f_d}{\partial \boldsymbol{\sigma}'} \right)^i : \boldsymbol{D} : \left(\frac{\partial f_d}{\partial \boldsymbol{\sigma}'} \right)^i \mathrm{d}\dot{\lambda}^i \Delta t + \left(\frac{\partial f_d}{\partial p_m^d} \frac{\partial p_m^d}{\partial \dot{\lambda}} \right)^i \mathrm{d}\dot{\lambda}^i + \left(\frac{\partial p_m^d}{\partial p_m^r} \frac{\partial p_m^r}{\partial \varepsilon_v^{vp}} \frac{\partial f_d}{\partial p'} \right)^i \mathrm{d}\dot{\lambda}^i \Delta t \end{aligned} \tag{30}$$

Based on it, the value of $\mathrm{d}\dot{\lambda}$ is computed by:

$$\mathrm{d}\dot{\lambda}^i = \frac{f_d^i}{\left(\frac{\partial f_d}{\partial \boldsymbol{\sigma}'} : \boldsymbol{D} : \frac{\partial f_d}{\partial \boldsymbol{\sigma}'} - \frac{\partial p_m^d}{\partial p_m^r} \frac{\partial p_m^r}{\partial \varepsilon_v^{vp}} \frac{\partial f_d}{\partial p'} \right)^i \Delta t - \left(\frac{\partial f_d}{\partial p_m^d} \frac{\partial p_m^d}{\partial \dot{\lambda}} \right)^i} \tag{31}$$

After calculating $\mathrm{d}\dot{\lambda}$, the stresses and hardening variables are updated by:

$$\boldsymbol{\sigma}'^{i+1} = \boldsymbol{\sigma}'^{i} - \mathrm{d}\dot{\lambda}^i \Delta t \boldsymbol{D} : \frac{\partial f_d}{\partial \boldsymbol{\sigma}'} \tag{32}$$

$$p_m^{d,i+1} = p_m^{d,i} + \left(\frac{\partial p_m^d}{\partial \dot{\lambda}} \right)^i \mathrm{d}\dot{\lambda}^i + \left(\frac{\partial p_m^d}{\partial p_m^r} \frac{\partial p_m^r}{\partial \varepsilon_v^{vp}} \frac{\partial f_d}{\partial p'} \right)^i \mathrm{d}\dot{\lambda}^i \Delta t \tag{33}$$

$$p_m^{r,i+1} = p_m^{r,i} + \left(\frac{\partial p_m^r}{\partial \varepsilon_v^{vp}} \right)^i \mathrm{d}\dot{\lambda}^i \Delta t \frac{\partial f_d}{\partial p'} \tag{34}$$

The integration process of the proposed MCP algorithm for one arbitrary loading step is

401 illustrated as follows:

(1) Calculate $\dot{\lambda}^0 = \mu(p_m^{d,0}/p_m^{r,0})^\beta$ and $\mathrm{d}\lambda^0 = \dot{\lambda}^0 \Delta t$, and then update σ'^{tr}, $p_m^{d,tr}$ and $p_m^{r,tr}$ by Eqs. (27)-(29).

(2) Check f_d^{tr}, enter iterative viscoplastic correction loop if $|f_d^{tr}| > FTOL$, otherwise complete the loading step.

(3) Calculate $\mathrm{d}\dot{\lambda}^i$ by Eq. (31) if $|f_d^{tr}| > FTOL$, and then update σ'^{i+1}, $p_m^{d,i+1}$ and $p_m^{r,i+1}$ by Eqs. (32)-(34).

(4) Check f_d^{i+1}, enter the next iterative viscoplastic correction loop if $|f_d^{i+1}| > FTOL$, otherwise complete the loading step.

402 For three-dimensional model, the flow direction of viscoplastic strain rate according to
403 the first-order derivative of dynamic loading surface is not constant. The extent of the flow
404 direction's change for a loading step should affect the performance of algorithm. For the
405 substepping procedure, therefore, the expression of distance between the trial stress and
406 dynamic loading surface adjusted on the predictor stage in one-dimensional condition is
407 modified to consider the change of flow direction, which is expressed by:

408 $$\mathrm{d}\bar{\boldsymbol{\sigma}}'^{tr} = \boldsymbol{\sigma}'^{tr} - \bar{\boldsymbol{\sigma}}' \tag{35}$$

409 where $\bar{\boldsymbol{\sigma}}'$ presents the image stress state defined by projecting the radial line that connects
410 the origin of coordinate and the initial stress state onto the dynamic loading surface adjusted
411 by predictor. According to this principle, the image stress could be determined by:

412 $$\bar{\boldsymbol{\sigma}}' = \frac{p_m^{d,tr}}{p_m^{d,0}} \boldsymbol{\sigma}'^0 \tag{36}$$

413 The adaptive substepping procedure for one loading step is then proposed for a given

substepping parameter k, shown as follows:

(1) Set initial value of $\alpha_j = 1$ for j = 1.

(2) Calculate $\boldsymbol{\sigma}'^{tr}_j$, $p^{d,tr}_{m,j}$ and $p^{r,tr}_{m,j}$ by using $\alpha_j \Delta\varepsilon$ and $\alpha_j \Delta t$, then calculate $\bar{\boldsymbol{\sigma}}'_j = (p^{d,tr}_{m,j} / p^{d,0}_{m,j})\boldsymbol{\sigma}'^{0}_j$.

(3) Compare $\mathrm{d}\bar{\boldsymbol{\sigma}}'^{tr}_j$ and $\boldsymbol{\sigma}'^{tr}_j$. If $\left\|\mathrm{d}\bar{\boldsymbol{\sigma}}'^{tr}_j\right\| / \left\|\boldsymbol{\sigma}'^{tr}_j\right\| > k$, α_j is adjusted by $\alpha_j = k\left\|\boldsymbol{\sigma}'^{tr}_j\right\| / \left\|\mathrm{d}\bar{\boldsymbol{\sigma}}'^{tr}_j\right\|$, and return back to (2) to re-calculate trial stresses and hardening variables.

(4) Calculate $\boldsymbol{\sigma}'_j$, $p^{d}_{m,j}$ and $p^{r}_{m,j}$ by viscoplastic correction.

(5) Check $\sum_j \alpha_j = 1$. If yes, the calculation is completed; otherwise, $\alpha_{j+1} = 1 - \Sigma\alpha_j$, return to (2).

To clarify the whole algorithm, the flow chart of the new MCP algorithm with the adaptive substepping technique for the three-dimensional condition is presented in Fig. 7.

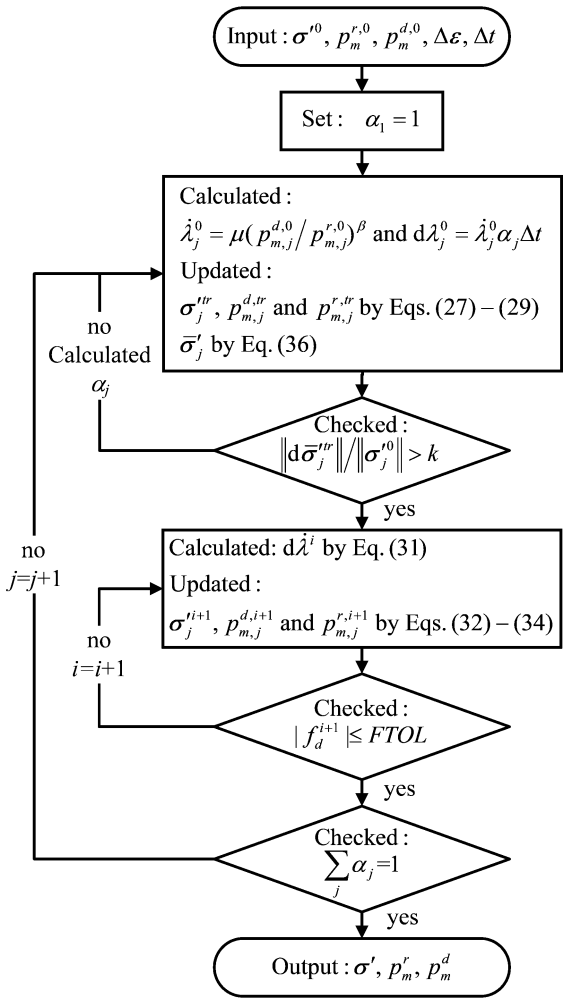

Figure 7 Flow chart of modified cutting-plane algorithm for three-dimensional EVP-MCC model

5 Numerical validations at integration point level

To analyse the accuracy and convergence of the proposed MCP time integration algorithm, a series of step-changed tests on Saint-Herblain clay[15,28] was simulated by the new integrated EVP-MCC model with all simulation results marked as "MCP" in figures. The EVP-MCC model by the new algorithm without substepping procedure (marked as "MCP-w/o") and by the original cutting-plane algorithm (marked as "OCP") were also used to simulate same tests for comparisons. This group of step-changed tests were well depicted by Yin et al..[15] The EVP-MCC model parameters are summarised in Table 1. To determine the relative error of calculated stress, the ''exact'' solution is obtained using the enough small

loading step size (e.g., 10^{-4} %). The relative error of stress is computed by:

$$Er = \sqrt{(E_p^2 + E_q^2)/2} \tag{37}$$

with

$$E_p = \sqrt{\sum_{i=1}^{N_c}\left(\frac{p_i' - p_{ex}'}{p_{ex}'}\right)^2 \Big/ N_c} \quad \text{and} \quad E_q = \sqrt{\sum_{i=1}^{N_c}\left(\frac{q_i - q_{ex}}{q_{ex}}\right)^2 \Big/ N_c} \tag{38}$$

where p_{ex}' and q_{ex} are the "exact" solutions; N_c represents the number of compared stress points.

5.1. Simulation of oedometer test

For the step-changed oedometer test, the initial vertical and radial stresses are 10 kPa and 4.9 kPa, respectively. The specimen was compressed to axial strains of 12 %, 15.5 % and 25 % in sequence with strain rates of 0.02 %/min, 0.004 %/min and 0.02 %/min, respectively. The step size of vertical strain $\Delta\varepsilon_z$ is in the range of 0.01 % to 1 %. The calculation results using MCP, MCP-w/o (i.e. MCP without substepping) and OCP are shown in Fig. 8. The substepping parameter *k* is set to 0.1, 0.2 and 0.5 respectively to examine the performance of the adaptive substepping technique.

Figs. 8(a)-(c) show good performance of MCP based on all calculations, except for the case of *k*=0.5 (Fig. 8(c)) with observing a calculation point at $\Delta\varepsilon_z$=1 % deviating from the exact solution during the abrupt decreasing of strain rate. This is because, according to the overstress theory, a significant viscoplastic strain could be generated for a given loading step size under the specific loading path, which leads to a reduction of accuracy and even failure of convergence.

Besides, Fig. 8(d) shows that the calculation by MCP-w/o cannot converge when $\Delta\varepsilon_z$ is

449 equal to 0.25 %. For this loading step size, the calculation results are far away from the exact
450 solution, even a negative vertical stress is obtained (which cannot be illustrated in the semi-
451 logarithmic coordinate) during the abrupt decreasing of strain rate due to the significant
452 viscoplastic strain rate. Fig. 8(e) shows that the calculation by OCP cannot converge when
453 $\Delta\varepsilon_z$ is equal to 0.5 %. The upper limit for loading step size to ensure the convergence of
454 OCP is larger than that of MCP-w/o. For this loading step size, the calculation cannot
455 converge due to large viscoplastic strain when the stress state is close to the normal
456 consolidation line.

457 The total iteration number *N* and the relative error of stress *Er* using MCP, MCP-w/o and
458 OCP are further compared in Fig. 9. The total iteration number of inelastic correction is the
459 sum of all sub-steps for all loading steps. For the model coded by MCP, the total iteration
460 number *N* decreases with the increasing of loading step size $\Delta\varepsilon_z$. It is mainly due to the
461 decreasing of total loading steps with the increasing of $\Delta\varepsilon_z$. The total iteration number *N*
462 with different *k* is similar when $\Delta\varepsilon_z$ is lower than or equal to 0.1 %. This is because the
463 substepping procedure is almost not activated. However, the total iteration number *N*
464 decreases more than 20 % from the case of *k*=0.1 to *k*=0.5 when $\Delta\varepsilon_z$ is larger than or equal to
465 0.25%. These results indicate that the substepping parameter *k* controls the substepping size
466 and affects the total iteration number. Besides, for the model coded by MCP, the relative error
467 of stress *Er* increases with the increasing of $\Delta\varepsilon_z$ and *k*. The relative error of stress *Er*
468 increases more or less twice from the case of *k*=0.1 to *k*=0.5 when $\Delta\varepsilon_z$ is larger than or equal
469 to 0.1 %.

For the model coded by MCP-w/o or OCP, as shown in Fig. 9, the total iteration number *N* also decreases and the relative error of stress *Er* increases with the increasing of loading step size $\Delta\varepsilon_z$. For the model coded by MCP-w/o, the total iteration number *N* is same as that by MCP with *k*=0.5 within the convergent range of $\Delta\varepsilon_z$. The relative error of stress *Er* calculated by MCP-w/o is also same as that by MCP with *k*=0.5. Both the comparisons of total iteration number *N* and relative error of stress *Er* between MCP-w/o and MCP with *k*=0.5 imply that the substepping procedure does not active for the case with low $\Delta\varepsilon_z$, which is reasonable since the low $\Delta\varepsilon_z$ implies a small incremental step.

The total iteration number *N* and the relative error of stress *Er* calculated by OCP are one order of magnitude larger than that by MCP for each $\Delta\varepsilon_z$. The poor performance of OCP is due to the inappropriate selecting of overstress stress function for Taylor series approximation. In this case, adopting an unreasonable target value of overstress function during viscoplastic correction loop leads to an abundant iteration process and an unacceptable calculated error, as discussed in section 2.

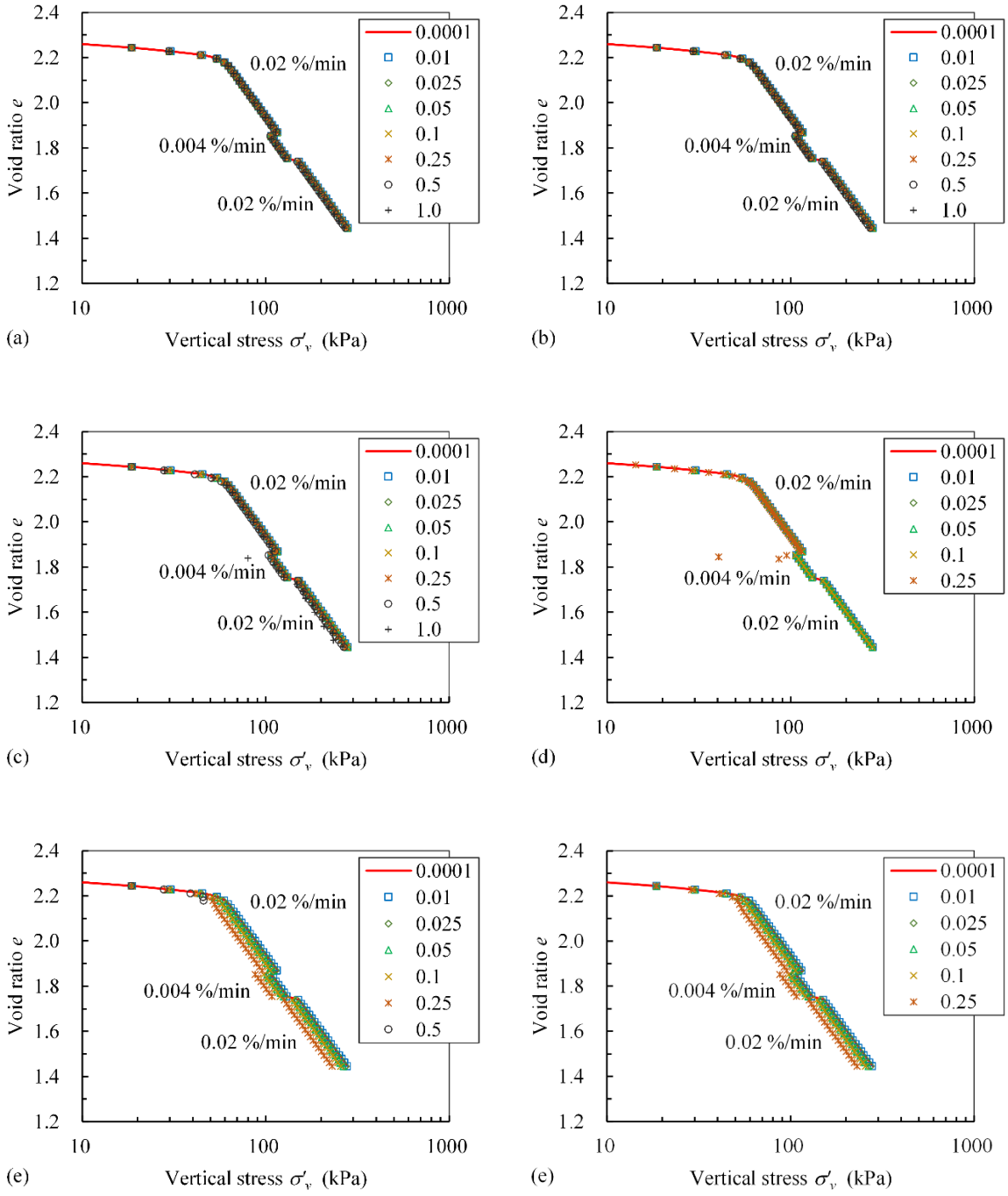

Figure 8 Simulations the step-changed oedometer test by MCP with (a) k=0.1, (b) k=0.2, and (c) k=0.5, (d) by MCP-w/o and (e) by OCP with different loading step size

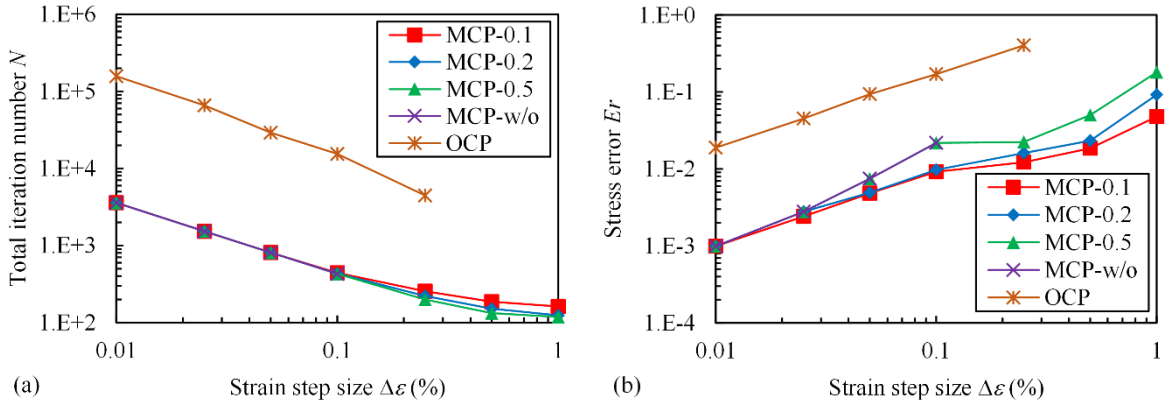

Figure 9 Comparison of (a) total iteration number and (b) relative error of stress using different integration methods with varied loading step size for the step-changed oedometer test

5.2. Simulation of undrained triaxial test

For the step-changed undrained triaxial test, the initial stress state of the specimen is same as that of oedometer test. The specimen was firstly compressed to the vertical stress of 86 kPa and the radial stress of 77 kPa within 24 hours. Then the specimen was sheared to axial strains of 2 %, 2.5 %, 4.7 % and 6.3 % in sequence with strain rates of 1 %/h, 0.1 %/h, 10 %/h and 0.1 %/h, respectively. The step size of axial strain $\Delta\varepsilon_a$ is in the range of 0.01 % to 1 %, and the substepping parameter k is set to 0.05, 0.1 and 0.15 respectively.

The calculation results using MCP and OCP are presented in Fig. 10. In this part the "MCP-w/o" is not included since the previous section has already identified the effective improvement due to the adaptive substepping. The calculations can converge for MCP with k=0.05, k=0.1 and k=0.15. However, the calculation cannot converge for MCP with k=0.2 at the abrupt decreasing of strain rate from 10 %/h to 0.1 %/h, even though the minimum strain step size, i.e. $\Delta\varepsilon_a$=0.01 %, is applied. Besides, the calculation by OCP cannot converge when $\Delta\varepsilon_a$ is equal to 1.0 %. For the case of $\Delta\varepsilon_a$=0.25 %, negative deviatoric stresses are calculated at the abrupt decreasing of strain rate from 10 %/h to 0.1 %/h; and for the case of

508 $\Delta\varepsilon_a$ =0.5 %, negative deviatoric stresses are calculated at the abrupt decreasing of strain rate
509 from 1 %/h to 0.1 %/h and from 10 %/h to 0.1 %/h. This phenomenon of non-convergence
510 and calculation errors at the abrupt decreasing of strain rate could be attributed to a
511 significant viscoplastic strain increment occurred.

512 The total iteration number *N* and the relative error of stress *Er* using MCP and OCP are
513 compared. Fig. 11(a) shows that the total iteration number *N* calculated by MCP decreases
514 with the increasing of $\Delta\varepsilon_a$ and *k* under triaxial stress path. The total iteration number *N*
515 decreases more than 30 % from the case of *k*=0.05 to *k*=0.15 when the $\Delta\varepsilon_a$ is larger than or
516 equal to 0.25%. Fig. 11(b) shows that the relative error of stress *Er* calculated by MCP
517 increases with the increasing of $\Delta\varepsilon_a$ and *k*. The relative error of stress *Er* increases more than
518 twice from the case of *k*=0.05 to *k*=0.15 for all the calculated range of $\Delta\varepsilon_a$.

519 As shown in Fig. 11, using the model coded by OCP, the total iteration number *N*
520 decreases and the relative error of stress *Er* increases with the increasing of $\Delta\varepsilon_a$, which are
521 generally larger than that calculated by MCP. The difference between the total iteration
522 number *N* calculated by OCP and that calculated by MCP decreases with the increasing of
523 $\Delta\varepsilon_a$, but the difference in stress error *Er* increases with the increasing of $\Delta\varepsilon_a$.

524 These comparisons for both oedometer and triaxial tests illustrate that the accuracy and
525 convergence rate of the MCP algorithms are dramatically enhanced, and the adaptive
526 substepping technique guarantees good performance despite large loading step size.

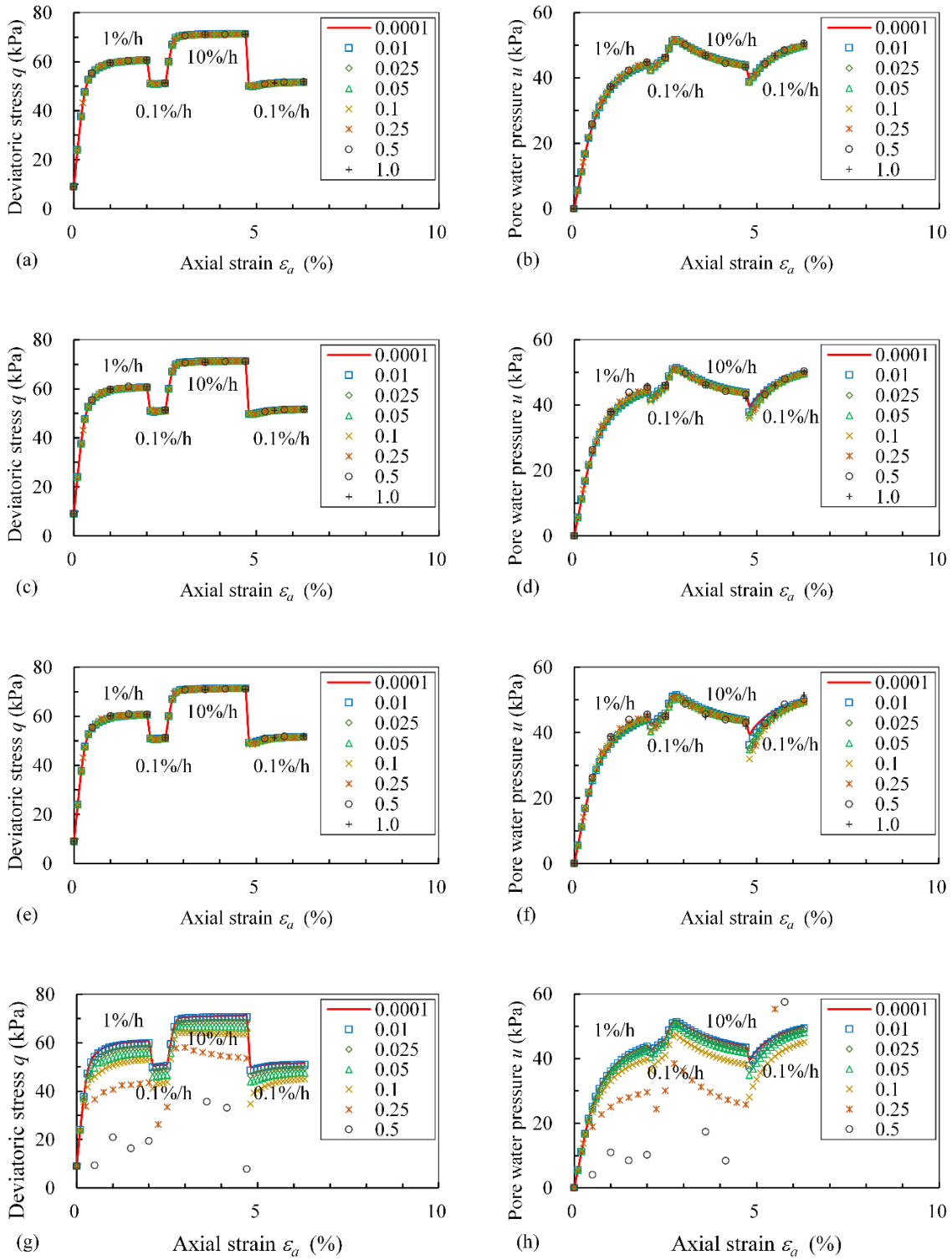

527

528

529

530

531 **Figure 10 Simulations the step-changed undrained triaxial test by MCP with k=0.05 for (a) q and (b) u,**
532 **k=0.1 for (c) q and (d) u, k=0.15 for (e) q and (f) u, and OCP for (g) q and (h) u with different loading step**
533 **size**

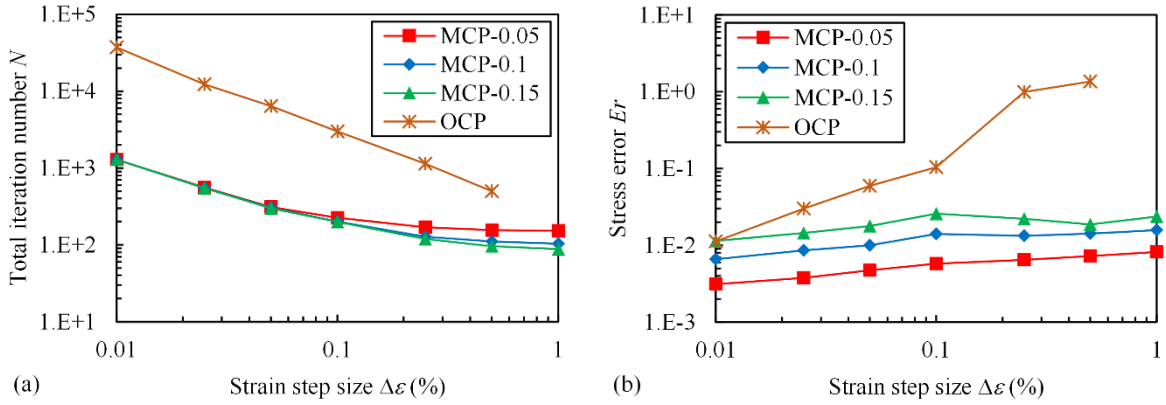

Figure 11 Comparison of (a) total iteration number and (b) relative error of stress using different integration methods with varied loading step size for the step-changed undrained triaxial test

6 Numerical validations at finite element level

A User Defined Soil Model (UDSM) for the EVP-MCC model has been developed using the proposed MCP algorithm via the commercial finite element code PLAXIS 2D. The model implementation followed the PLAXIS material models manual[31] for implementing user-defined constitutive models.

In order to purely examine the performance of the MCP, a series of numerical plane strain biaxial shear tests was simulated using MCP-integrated model in PLAXIS to illustrate the variations of global iteration number and global calculation time with effects of mesh density and substepping parameter *k*. Note that the OCP-integrated model was also implemented into PLAXIS and used to simulate tests, but all simulations cannot converge. Parameters of EVP-MCC model are the same as that used in previous numerical validations at integration point level.

In the plane strain test, the size of the sample is 0.3 m long and 0.6 m high. The bottom boundary displacement is restrained in both the vertical and horizontal directions, and the top

boundary displacement is restrained only in the horizontal direction. On the lateral boundary the displacement is not restrained in both the vertical and horizontal directions. The 6-noded triangular element was selected to generate meshes.

The plane strain biaxial shear tests of normally consolidated soil (over-consolidation ratio OCR = 1) and over-consolidated soil (OCR = 8) were simulated. For the shear test of normally consolidated soil, the simulation was conducted in two stages. The sample was first isotropically compressed to a target stress of 50 kPa within one hour, followed by a creep stage of 24 hours. Then, the top side of the sample was loaded to a vertical displacement of 0.09 m by displacement control at a global vertical strain rate of 0.1 %/h. For the shear test of over-consolidated soil, the simulation was conducted in six stages. The sample was incrementally compressed to target stresses of 50, 100, 200 and 400 kPa, within one hour for each and followed by a creep stage of 24 hours for each. Then, the sample was unloaded to a target stress of 50 kPa within 24 hours. Finally, the top side of the sample was loaded to a vertical displacement of 0.09 m by displacement control at a global vertical strain rate of 0.1 %/h. All simulations were conducted up to a global strain of 15% with a total step number around 30.

6.1. Effect of mesh density

Fine, middle and coarse densities of finite element mesh were chosen to examine the performance of MCP in terms of mesh-dependency by simulating plane strain tests. The corresponding numbers of elements are 592, 268 and 98, respectively for different mesh densities. The value of substepping parameter k is set to 0.1 according to above studies to

guarantee the convergence.

The comparisons of total number of iteration and CPU time for test simulations of normally consolidated and over-consolidated soils with different mesh densities by the MCP-integrated model are summarised in Table 2. The variation of global iteration number is slight for both soils. The global iteration number slightly decreases with the decreasing of the element number for the normally consolidated soil, however, the variation of global iteration number is non-monotonic with the element number for the over-consolidated soil. The CPU time decreases with the decreasing of mesh density, and the CPU time with fine mesh density is almost two or three times than that with middle and coarse densities for both soils.

Table 2. Total number of iteration and CPU time for different mesh densities

OCR	Comparison items	Total element number		
		of 592 (fine)	of 268 (middle)	of 98 (coarse)
1	Number of iteration	598	579	559
	CPU time (s)	7.23	3.65	3.12
8	Number of iteration	1666	1533	1606
	CPU time (s)	16.47	6.75	4.95

The simulated results of MCP for both soils are illustrated in Fig. 12, which shows a mesh-independent curve of global $\varepsilon_y - \sigma_y$ (ε_y defined as the total vertical displacement of top surface over initial height of the sample; σ_y defined as the total forces at top surface over the area of top surface). The deviatoric strain fields for fine, middle and coarse mesh densities are shown in Fig. 13 for normally consolidated soil and Fig. 14 for over-consolidated soil, which also reveals mesh-independency of the simulation when using elasto-viscoplastic models in finite element analysis.

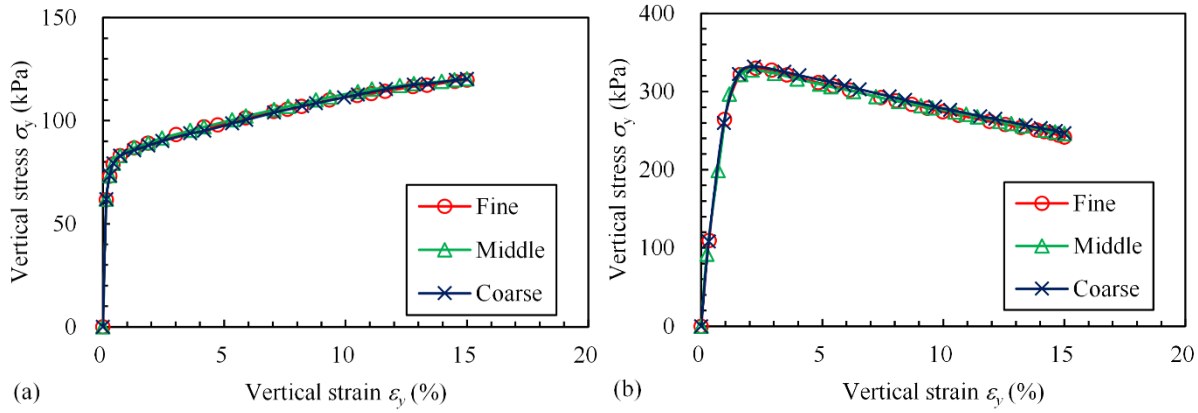

591

592 **Figure 12 Comparison of simulated results with different mesh densities for biaxial shear test of (a)**
593 **normally consolidated soil and (b) over-consolidated soil**

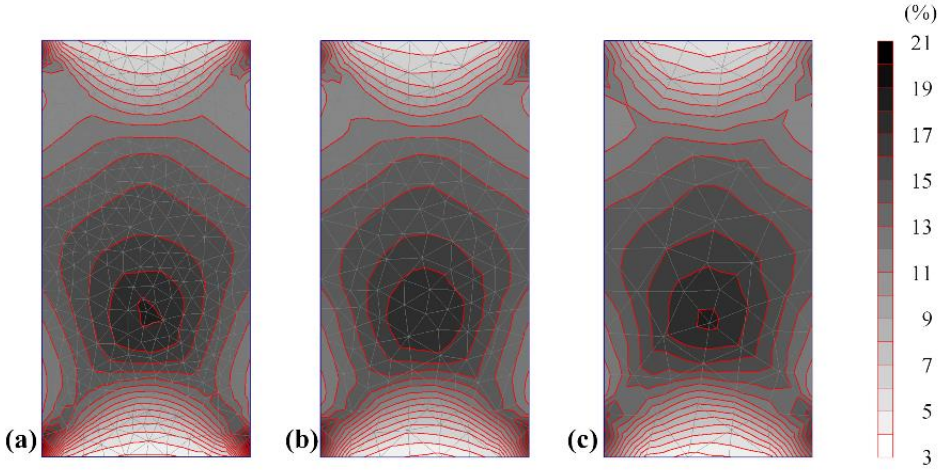

594

595 **Figure 13 Comparison of deviatoric strain fields simulated with (a) fine (b) middle and (c) coarse mesh**
596 **densities for biaxial shear test of normally consolidated soil**

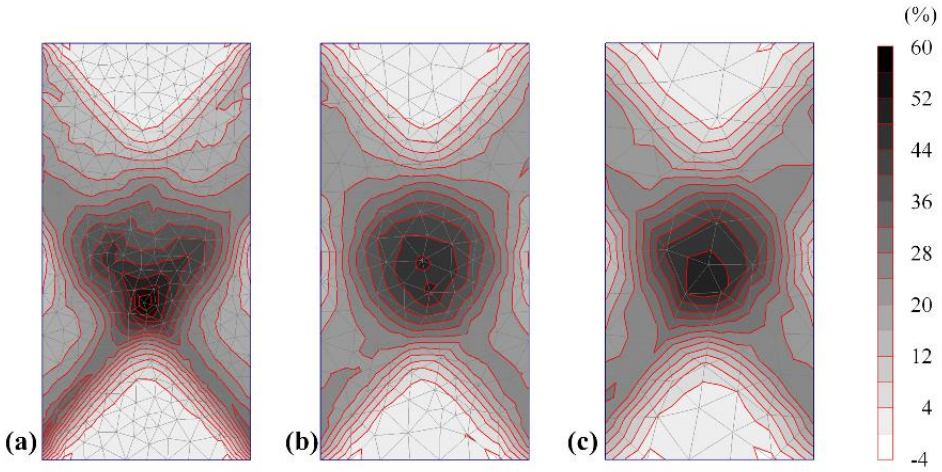

597

598 **Figure 14 Comparison of deviatoric strain fields simulated with (a) fine (b) middle and (c) coarse mesh**
599 **densities for biaxial shear test of over-consolidated soil**

6.2. Effect of substepping parameter k

The results of numerical validations at integration point level illustrated that the performance of the proposed MCP algorithm becomes worse with the increasing of substepping parameter which controls the substepping size. To analyse the effect of substepping parameter *k* at finite element level, simulations of the plane strain tests by the MCP-integrated model with different *k* (0.1, 0.2 and 0.5, respectively) were carried out. Only the fine mesh was selected to highlight the impact of substepping parameter.

The comparisons of total number of iteration and CPU time for all test simulations of normally consolidated soil and over-consolidated soil by the MCP-integrated model with different *k* are summarised in Table 3. The global iteration number and the CPU time slightly increase with the increasing of substepping parameter *k* for both soils except that the CPU time for the simulations over-consolidated soil with $k = 0.2$ is slightly larger than that with $k = 0.5$.

Table 3. Total number of iteration and CPU time for different values of *k*

OCR	Comparison items	Substepping parameter *k*		
		of 0.1	of 0.2	of 0.5
1	Number of iteration	598	633	682
	CPU time (s)	7.23	7.78	8.31
8	Number of iteration	1666	1888	1898
	CPU time (s)	16.47	18.06	17.86

The simulated results of global $\varepsilon_y - \sigma_y$ response by MCP for both soils are illustrated in Fig. 15. Fig. 15(a) illustrates that the simulated curves of normally consolidated soil are consistent each other. As shown in Fig. 15(b), the $\varepsilon_y - \sigma_y$ curve of the over-consolidated soil

simulated by MCP with k =0.5 are lower than those calculated by MCP with k =0.1 and 0.2 when the value of vertical strain exceeds 10%. It implies that the softening phenomenon was overestimated due to the calculated stress errors for the case simulated by MCP with k =0.5, since a higher value of k corresponding to a bigger sub-step size may result in a higher error which agrees with the previous results at the level of integration point (simulated results for oedometer and triaxial tests).

For normally consolidated soil, the deviatoric strain field for k = 0.2 is examined the same as that of k = 0.1, shown in Fig. 16(a) and (b). However, as shown in Fig. 16(c), the field of deviatoric strain, calculated by MCP with k = 0.5, there is one gauss point at the lower left-hand of the soil sample with higher strain level (ε_d = 35%) than those (ε_d = 21%) calculated by MCP with k = 0.1 and 0.2, which could be attributed to the calculated error of stress at this stress integrated point by k = 0.5 significantly higher than that by k = 0.1 and 0.2. However, the global stress-strain response is not influenced since only one gauss point has different results.

For over-consolidated soil as shown in Fig. 17, the field of deviatoric strain, calculated by MCP with k =0.5, is globally greater than those calculated by MCP with k =0.1 and 0.2 along the shear band of the soil sample, which also could be attributed to the higher calculated error of stress at stress integrated points when using k = 0.5 compared to k = 0.1 and 0.2. It can be concluded that the simulation with k =0.5 can get convergence but not accuracy.

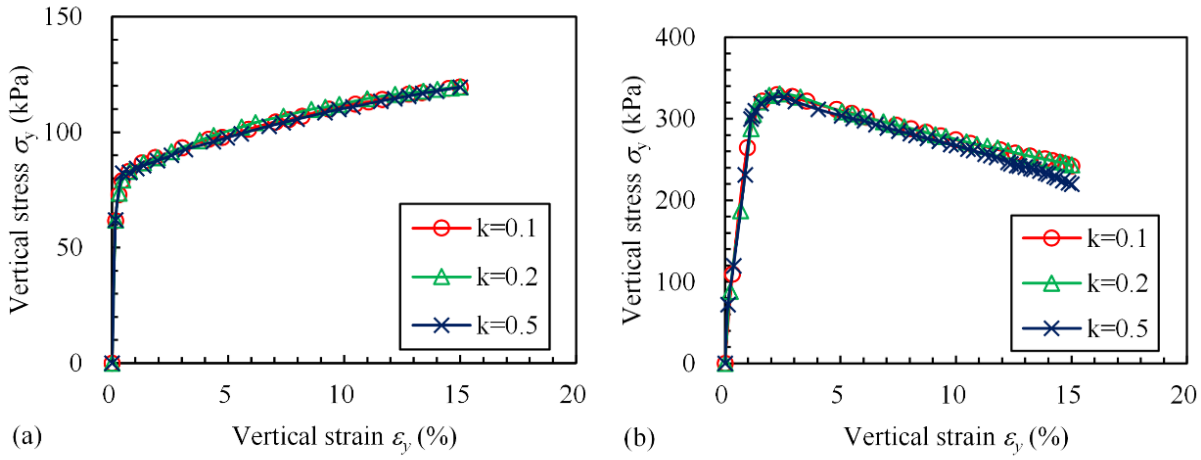

642
643 **Figure 15 Comparison of simulations with different mesh densities for biaxial shear test of (a) normally**
644 **consolidated soil and (b) over-consolidated soil**

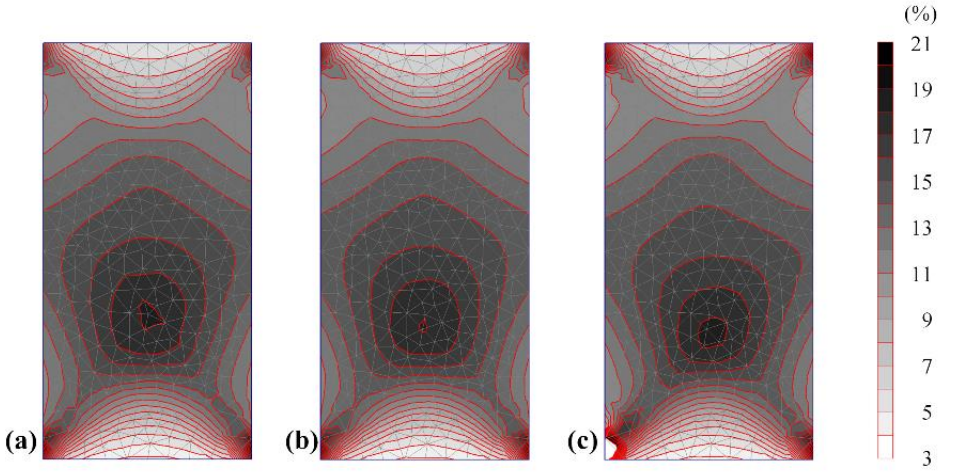

645
646 **Figure 16 Comparison of deviatoric strain fields simulated with (a) k=0.1 (b) k=0.2 and (c) k=0.5 for**
647 **biaxial shear test of normally consolidated soil**

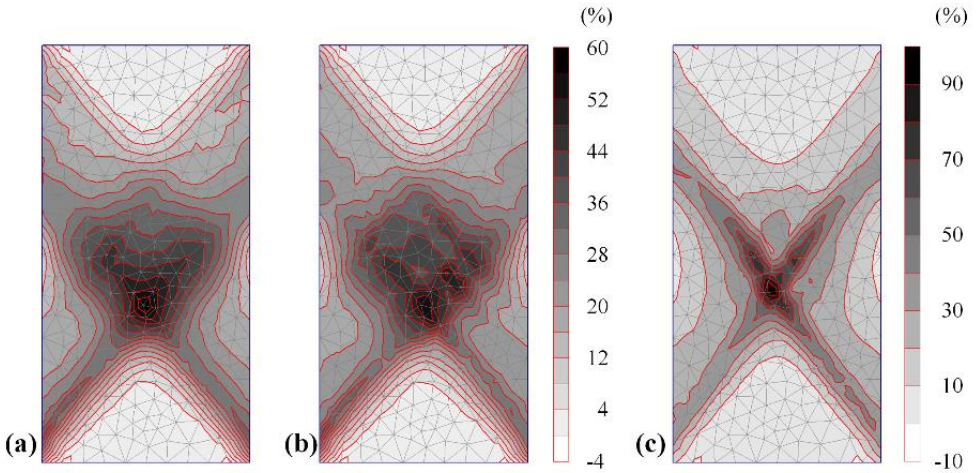

648
649 **Figure 17 Comparison of deviatoric strain fields simulated with (a) k=0.1 (b) k=0.2 and (c) k=0.5 for**
650 **biaxial shear test of over-consolidated soil**

7 Conclusions

A novel adaptive substepping cutting-plane time integration scheme (MCP) keeping the advantage of original cutting-plane algorithm (OCP) with only the first derivatives of loading surface required was proposed for elasto-viscoplastic models. The performance of the original cutting-plane algorithm (OCP) for the elasto-viscoplastic model EVP-MCC was first identified poor due to the particularity of viscoplastic formulation. To overcome this, an evolution function for the hardening variable of dynamic loading surface is innovatively deduced for the Taylor series approximation, the elastic predictor is modified to account for the initial viscoplastic strain rate with more accuracy, and a new adaptive substepping technique for restricting simultaneously both strain and time incremental sizes based on the overstress distance is proposed. For easy understanding, the proposed algorithm is first presented for one-dimensional condition, and then extended to three-dimensional condition.

The new integrated EVP-MCC model using the proposed algorithm is examined by simulating laboratory tests at both levels of integration point and finite element method. At the integration point level, a group of step-changed tests was selected to examine the performance of MCP. The total iteration number decreases with the decreasing of loading step size and the increasing of substepping parameter *k*. The relative error of stress increases with the increasing of the loading step size and the substepping parameter *k*. All of them are remarkably lower than that using OCP because of an unreasonable target value of overstress function during plastic correction loop adopted in OCP. At the finite element level, the MCP was validated by simulating a numerical plane strain biaxial shear test of normally

672 consolidated soil and over-consolidated soil. The variation of global iteration number with
673 mesh densities is slight. However, the CPU time decreases with the decreasing of element
674 number. Moreover, the variations of global iteration number and CPU time with substepping
675 parameter k are slight. However, the simulation using k = 0.5 for both soils can get
676 convergence but not accuracy, which could be attributed to the calculated error of stress at
677 some stress integrated points.

678 All comparisons comprehensively demonstrate that the performance of MCP with
679 substepping technique is good for both the integration point level and the finite element level.
680 The MCP should be thus applicable and recommended for elasto-viscoplastic models in finite
681 element analysis.

682 ## Acknowledgments

683 We acknowledge with gratitude the financial support provided by a RIF project (PolyU
684 R5037-18F) from Research Grants Council (RGC) of Hong Kong Special Administrative
685 Region Government (HKSARG) of China, and the Fundamental Research Funds for the
686 Central Universities (2019JBM083).

687

688

Appendix A: brief introduction of three-dimensional EVP-MCC model

The EVP-MCC model is based on the overstress theory[20,21] and the modified Cam-Clay model[32]. According to the section 2.1, complementary equations are summarized as follows:

$$\Phi = \left(\frac{p_m^d}{p_m^r} \right)^{\beta} \tag{A.1}$$

$$\beta = \frac{\lambda - \kappa}{C_{\alpha e}}, \quad \mu = \frac{C_{\alpha e}}{\tau_r (1+e_0)(1-\eta_{K0}^2 / M_c^2)} \tag{A.2}$$

$$f_d = \frac{\frac{3}{2}\boldsymbol{\sigma}_d' : \boldsymbol{\sigma}_d'}{M^2 p'} + p' - p_m^d = 0 \tag{A.3}$$

$$M = M_c \left[\frac{2c^4}{1 + c^4 + (1-c^4)\sin 3\theta} \right]^{\frac{1}{4}} \tag{A.4}$$

$$\mathrm{d}p_m^r = p_m^r \frac{1+e_0}{\lambda - \kappa} \mathrm{d}\varepsilon_v^{vp} \tag{A.5}$$

where p_m^d and p_m^r are the sizes of the dynamic loading surface and the reference surface, respectively (see Fig. A.1); β is the strain-rate coefficient; λ is the slope of the normal compression line; κ is the slope of the swelling line; $C_{\alpha e}$ is the secondary compression coefficient; τ_r is the duration of incremental loading used in the conventional oedometer test with a common value of 24 h; e_0 is the initial void ratio; η_{K0} is the stress ratio under the condition of K_0-consolidation with $\eta_{K0} = (\sqrt{9 + 4M_c^2} - 3)/2$ according to the stress-dilatancy relationship of the modified Cam-Clay model; M is the slope of CSL in the p'-q plane, i.e., mean effective stress – deviatoric stress plane; $c=M_e/M_c$ with the slope of CSL in triaxial compression and extension, i.e., M_c and M_e, respectively; θ is lode angle, and $-\pi/6 \le \theta = (1/3)\sin^{-1}(-3\sqrt{3}J_3 / 2J_2^{3/2}) \le \pi/6$ with the second and third invariants of deviator stress tensor, i.e., J_2 and J_3, respectively; $\boldsymbol{\sigma}_d'$ is the deviatoric stress tensor expressed by $\boldsymbol{\sigma}_d' = [\sigma_x' - p', \sigma_y' - p', \sigma_z' - p', \sqrt{2}\tau_{xy}, \sqrt{2}\tau_{yz}, \sqrt{2}\tau_{zx}]^T$; the effective stress tensor $\boldsymbol{\sigma}'$ is expressed by $\boldsymbol{\sigma}' = [\sigma_x', \sigma_y', \sigma_z', \tau_{xy}, \tau_{yz}, \tau_{zx}]^T$ and the mean effective stress p' is defined by $p' = (\sigma_x' + \sigma_y' + \sigma_z')/3$; ε_v^{vp} is the volumetric viscoplastic strain. The determination methods for all these parameters of EVP-MCC model are summarised in Table A.1.

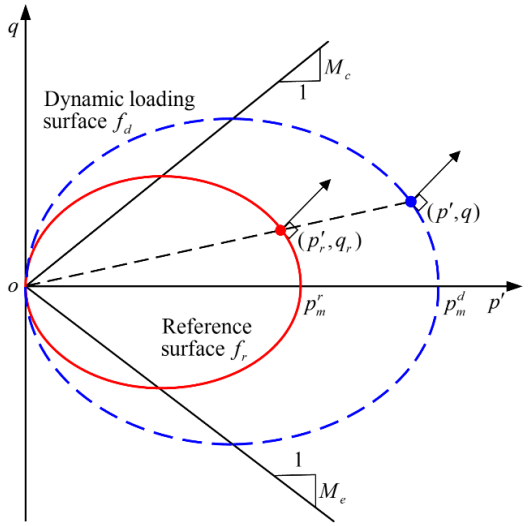

Figure A.1 Principle of EVP-MCC model

Table A.1 State parameters and constants of EVP-MCC model

Type	Parameter	Definition	Determination
Modified Cam-Clay parameters	p^r_{m0}	Initial size of reference surface	From a oedometer test corresponding to a given reference strain-rate or reference time
	e_0	Initial void ratio	From physical properties of the soil
	υ	Poisson's ratio	From initial part of stress-strain curve
	κ	Swelling index	From oedometer test or consolidation test
	λ	Compression index	From oedometer test or consolidation test
	M_c	Slope of CSL in triaxial compression	From triaxial shear test
Viscosity parameter	$C_{\alpha e}$	Secondary compression coefficient	From conventional oedometer test

Appendix B: EVP-MCC induced one-dimensional model

The EVP-MCC model is reduced for one-dimensional condition, for which complementary equations are summarized as follows:

$$\Phi = \left(\frac{\sigma_p^d}{\sigma_p^r} \right)^{\beta} \tag{A.6}$$

$$f_d = \sigma' - \sigma_p^d = 0 \tag{A.7}$$

$$\mathrm{d}\sigma_p^r = \sigma_p^r \frac{1+e_0}{\lambda-\kappa} \mathrm{d}\varepsilon^{vp} \tag{A.8}$$

where σ_p^d and σ_p^r are the sizes of the dynamic loading surface and the reference surface, respectively, for one-dimensional condition; σ' is the effective stress; ε^{vp} is the viscoplastic strain.

References

1. Graham J, Crooks JHA, Bell AL. Time effects on the stress-strain behaviour of natural soft clays. *Géotechnique*. 1983;33(3):327-40.
2. Leroueil S, Kabbaj M, Tavenas F, Bouchard R. Stress-strain-strain rate relation for the compressibility of sensitive natural clays. *Géotechnique*. 1985;35(2):159-80.
3. Sheahan TC, Ladd CC, Germaine JT. Rate-dependent undrained shear behaviour of saturated clay. *J Geotech Engrg (ASCE)*. 1996;122(2):99-108.
4. Wang L, Dan H, Li L. Modelling strain-rate dependent behavior of KR_0-consolidated soft clays. *J Eng Mech (ASCE)*. 2012;138(7):738-48.
5. Yin Z-Y, Zhu Q-Y, Yin J-H, Ni Q. Stress relaxation coefficient and formulation for soft soils. *Geotech Lett*. 2014;4(1):45-51.
6. Yao YP, Kong LM, Zhou AN, Yin JH. Time-dependent unified hardening model: three-dimensional elasto-visco-plastic constitutive model for clays. *J Eng Mech (ASCE)*. 2015;141(6):0414162.
7. Yin Z-Y, Zhu Q-Y, Zhang D-M. Comparison of two creep degradation modeling approaches for soft structured soils. *Acta Geotech*. 2017;12(6):1395-413.
8. Hinchberger SD, Rowe RK. Evaluation of the predictive ability of two elastic-viscoplastic constitutive models. *Can Geotech J*. 2005;42(6):1675-94.
9. Karstunen M, Yin Z-Y. Modelling time-dependent behaviour of Murro test embankment. *Géotechnique*. 2010;60(10):735-49.
10. Yin Z-Y, Yin J-H, Huang H-W. Rate-dependent and long-term yield stress and strength of soft Wenzhou marine clay: experiments and modeling. *Mar Georesour Geotec*. 2015;33(1):79-91.
11. Rezania M, Taiebat M, Poletti E. A viscoplastic SANICLAY model for natural soft soils. *Comput Geotech*. 2016;73:128-41.
12. Katona MG. Evaluation of viscoplastic cap model. *J Geotech Engrg (ASCE)*. 1984;110(8):1106-25.

13. Ortiz M, Simo JC. An analysis of a new class of integration algorithms for elastoplastic constitutive relations. *Int J Numer Meth Engng*. 1986;23(3):353-66.
14. Stolle DFE, Vermeer PA, Bonnier PG. Time integration of a constitutive law for soft clays. *Commun Numer Meth Engng*. 1999;15(8):603-9.
15. Yin Z-Y, Chang CS, Karstunen M, Hicher P-Y. An anisotropic elastic-viscoplastic model for soft clays. *Int J Solids Struct*. 2010;47(5):665-77.
16. Higgins W, Chakraborty T, Basu D. A high strain-rate constitutive model for sand and its application in finite-element analysis of tunnels subjected to blast. *Int J Numer Anal Meth Geomech*. 2013;37(15):2590-610.
17. Yin Z-Y, Karstunen M, Wang J H, Yu C. Influence of features of natural soft clay on the behavior of embankment. *J Cent South Univ Techno*l. 2011;18(5):1667-1676.
18. Yin Z-Y, Xu Q, Yu C. Elastic-viscoplastic modeling for natural soft clays considering nonlinear creep. *Int J Geomech*. 2014;15(5):A6014001.
19. Yin Z-Y, Li J, Jin Y-F, Liu F-Y. Estimation of robustness of time integration algorithms for elasto-viscoplastic modeling of soils. *Int J Geomech*. 2019;19(2):04018197.
20. Perzyna P. The constitutive equations for work-hardening and rate sensitive plastic materials. *Proc Vibr Probl Warsaw*. 1963;3:281-90.
21. Perzyna P. Fundamental problems in viscoplasticity. *Adv Appl Mech*. 1966;9:243-377.
22. Borja RI, Lee SR. Cam-clay plasticity, part 1: implicit integration of elasto-plastic constitutive relations. *Comput Methods Appl Mech Engrg*. 1990;78(1):49-72.
23. Bushnell D. A strategy for the solution of problems involving large deflections, plasticity and creep. *Int J Numer Meth Eng*. 1977;11:683-708.
24. Schreyer HL, Kulak RF, Kramer JM. Accurate numerical solutions for elasto-plastic models. *J Press Vess-T ASME*. 1979;101:226-34.
25. Wang W, Datcheva M, Schanz T, Kolditz O. A sub-stepping approach for elastoplasticity with rotational hardening. *Comput Mech*. 2006;37:266-78.
26. Sloan SW. Substepping schemes for the numerical integration of elastoplastic stress-strain relations. *Int J Numer Meth Eng*. 1987;24(5):893-911.

27. Sloan SW, Abbo AJ, Sheng DC. Refined explicit integration of elastoplastic models with automatic error control. *Eng Computation*. 2001;18(1/2):121-94.
28. Yin Z-Y, Hicher P-Y. Identifying parameters controlling soil delayed behaviour from laboratory and in situ pressuremeter testing. *Int J Numer Anal Meth Geomech*. 2008;32(12):1515-1535.
29. Yin Z-Y, Karstunen M, Hicher PY. Evaluation of the influence of elasto-viscoplastic scaling functions on modelling time-dependent behaviour of natural clays. *Soils Found*. 2010;50(2):203-214.
30. Yin Z-Y, Karstunen M, Chang CS, Koskinen M, Lojander M. Modeling time-dependent behavior of soft sensitive clay. *J Geotech Geoenviron Eng ASCE*. 2011;137(11):1103-1113.
31. Plaxis. PLAXIS material models manual. Delft; 2012.
32. Roscoe KH, Burland JB. On the generalised stress-strain behaviour of 'wet' clay. In: Heyman J, Leckie FA, ed. *Engineering Plasticity*. Cambridge: Cambridge University Press; 1968:535-609.